Cell Reports

Article

ZEB1 shapes AML immunological niches, suppressing CD8 T cell activity while fostering Th17 cell expansion

Graphical abstract

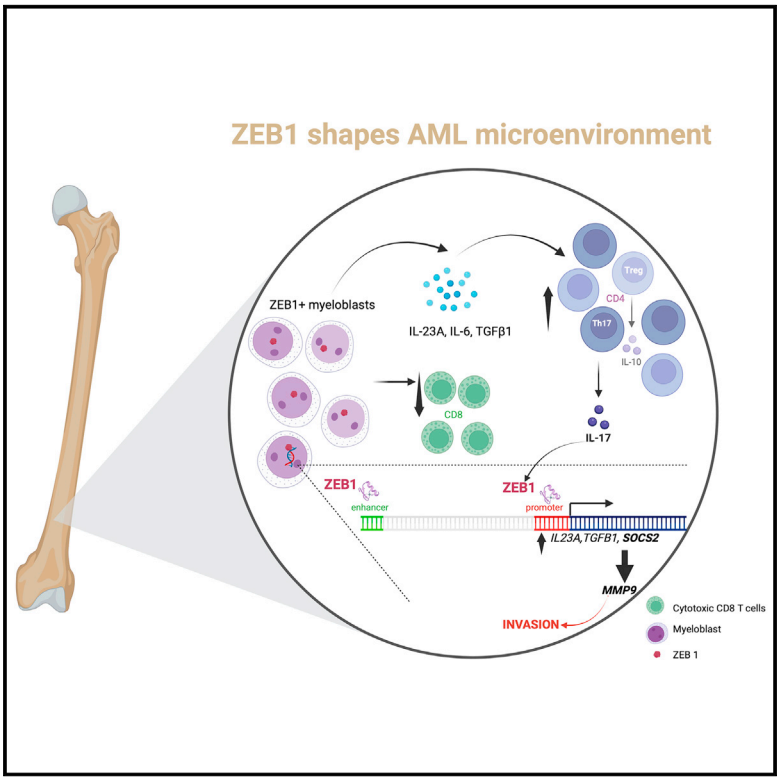

Highlights

- ZEB1+ AML blasts are immune regulatory via Th17 expansion
- IL-17 promotes proliferation and invasion of ZEB1+ cells
- IL-17 promotes ZEB1 binding to target gene promoters
- ZEB1 blast features combine immune regulation and chemoresistance

Authors

Barbara Bassani, Giorgia Simonetti, Valeria Cancila, ..., Claudio Tripodo, Mario P. Colombo, Sabina Sangaletti

Correspondence

mariopaolo.colombo@istitutotumori.mi.it (M.P.C.), sabina.sangaletti@istitutotumori.mi.it (S.S.)

In brief

Bassani et al. show that ZEB1 drives immune suppression and pro-tumoral Th17 cell development in AML. Silencing ZEB1 in leukemic cells limits disease in mice. Clinical data identify a ZEB1^{high} patient subgroup with poor outcomes, unveiling its significance in AML progression as both a pro-tumoral and immune regulatory factor.

Bassani et al., 2024, Cell Reports *43*, 113794
February 27, 2024
https://doi.org/10.1016/j.celrep.2024.113794

CellPress

Cell Reports

CellPress
OPEN ACCESS

Article

ZEB1 shapes AML immunological niches, suppressing CD8 T cell activity while fostering Th17 cell expansion

Barbara Bassani,[1] Giorgia Simonetti,[2] Valeria Cancila,[3] Antonio Fiorino,[4] Marilena Ciciarello,[5,6,7] Annamaria Piva,[1] Arman Mandegar Khorasani,[1] Claudia Chiodoni,[1] Daniele Lecis,[1] Alessandro Gulino,[8] Eugenio Fonzi,[9] Laura Botti,[1] Paola Portararo,[1] Massimo Costanza,[10] Marta Brambilla,[11] Giorgia Colombo,[12] Juerg Schwaller,[13] Alexandar Tzankov,[14] Maurilio Ponzoni,[15] Fabio Ciceri,[15] Niccolò Bolli,[16,17] Antonio Curti,[18] Claudio Tripodo,[3,19] Mario P. Colombo,[1,*] and Sabina Sangaletti[1,20,*]

[1]Molecular Immunology Unit, Department of Experimental Oncology, Fondazione IRCCS Istituto Nazionale Tumori, Milan, Italy
[2]Biosciences Laboratory, IRCCS Istituto Romagnolo per lo Studio dei Tumori (IRST) "Dino Amadori", Meldola, Italy
[3]Tumor Immunology Unit, Department of Health Sciences, Human Pathology Section, School of Medicine, University of Palermo, 90133 Palermo, Italy
[4]Predictive Medicine: Molecular Bases of Genetic Risk Unit, Department of Experimental Oncology, Fondazione IRCCS Istituto Nazionale Tumori, Milan, Italy
[5]CNR Institute of Molecular Genetics "Luigi Luca Cavalli-Sforza," Unit of Bologna, Bologna, Italy
[6]IRCCS Istituto Ortopedico Rizzoli, Bologna, Italy
[7]Department of Medical and Surgical Sciences (DIMEC), University of Bologna, Bologna, Italy
[8]CGT Lab, Cogentech Società Benefit, Catania, Italy
[9]Unit of Biostatistics and Clinical Trials, IRCCS Istituto Romagnolo per lo Studio dei Tumori (IRST) "Dino Amadori," Meldola, Forlì-Cesena, Italy
[10]Neuro-Oncology Unit, Department of Clinical Neuroscience, Fondazione IRCCS Istituto Neurologico Carlo Besta, Milan, Italy
[11]Medical Oncology Department, Fondazione IRCCS Istituto Nazionale dei Tumori, Milan, Italy
[12]Department of Pharmaceutical Sciences, Università del Piemonte Orientale, Novara, Italy
[13]University Children's Hospital Basel & Department of Biomedicine, University of Basel, Basel, Switzerland
[14]Institute of Medical Genetics and Pathology, University Hospital Basel, University of Basel, Basel, Switzerland
[15]IRCCS Ospedale S. Raffaele, University Vita-Salute San Raffaele, Milan, Italy
[16]Hematology Division, Foundation IRCCS Ca' Granda Ospedale Maggiore Policlinico, 20122 Milan, Italy
[17]Department of Oncology and Hemato-Oncology, University of Milan, 20122 Milan, Italy
[18]Department of Experimental, Diagnostic and Specialty Medicine – DIMES, Institute of Hematology "Seràgnoli," Bologna, Italy
[19]IFOM-ETS-The AIRC Institute of Molecular Oncology, Milan, Italy
[20]Lead contact
*Correspondence: mariopaolo.colombo@istitutotumori.mi.it (M.P.C.), sabina.sangaletti@istitutotumori.mi.it (S.S.)
https://doi.org/10.1016/j.celrep.2024.113794

SUMMARY

Acute myeloid leukemia (AML) progression is influenced by immune suppression induced by leukemia cells. ZEB1, a critical transcription factor in epithelial-to-mesenchymal transition, demonstrates immune regulatory functions in AML. Silencing *ZEB1* in leukemic cells reduces engraftment and extramedullary disease in immune-competent mice, activating CD8 T lymphocytes and limiting Th17 cell expansion. ZEB1 in AML cells directly promotes Th17 cell development that, in turn, creates a self-sustaining loop and a pro-invasive phenotype, favoring transforming growth factor β (TGF-β), interleukin-23 (IL-23), and SOCS2 gene transcription. In bone marrow biopsies from AML patients, immunohistochemistry shows a direct correlation between ZEB1 and Th17. Also, the analysis of ZEB1 expression in larger datasets identifies two distinct AML groups, *ZEB1*^{high} and *ZEB1*^{low}, each with specific immunological and molecular traits. *ZEB1*^{high} patients exhibit increased IL-17, SOCS2, and TGF-β pathways and a negative association with overall survival. This unveils *ZEB1*'s dual role in AML, entwining pro-tumoral and immune regulatory capacities in AML blasts.

INTRODUCTION

The bone marrow (BM) is a peculiar primary lymphoid organ in which the recirculation of naive T cells and the presence of antigen-presenting cells competent for presentation may trigger anti-leukemia T cell responses. Along this line, the number of T cells, present in the BM at diagnosis, correlates with overall survival (OS) in patients with newly diagnosed acute myeloid leukemia (AML).[1–3] Progression seen in AML suggests that immune suppressive mechanisms should be in place, overcoming anti-tumor

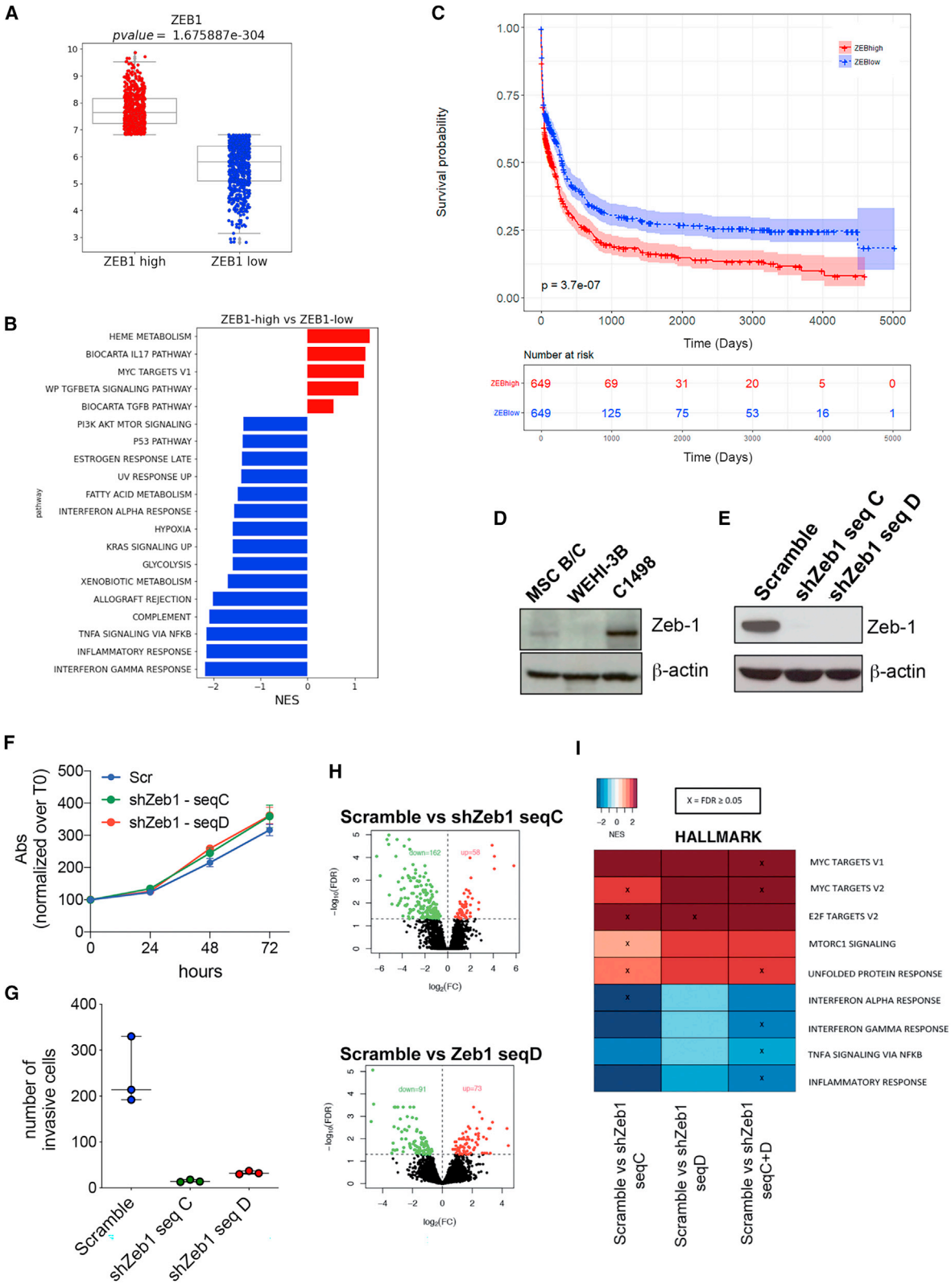

(legend on next page)

T cell responses. In the hematopoietic niche, leukemic cells interact with BM stromal cells, establishing favorable conditions for survival, proliferation, and resistance to therapy as well as escape from immune recognition.[4,5] As reported in solid tumors, potentially immunogenic leukemia cells seem to develop multiple mechanisms for immune escape including the establishment of immune suppression. These different immunomodulatory mechanisms encompass regulatory T (Treg) cells, myeloid-derived suppressor cells,[6] engagement of inhibitory T cell pathways (i.e., PD-L1-/PD-1, arginase [Arg]-2),[7,8] or interference with specific metabolic pathways through indoleamine-2,3-dioxygenase.[9] The engagement of bystander cells, such as BM mesenchymal stromal cells, or a direct endogenous activity of AML blast seems necessary to produce key factors capable of regulating immune cell activities.

ZEB1 has been extensively studied in solid cancers as a main transcription factor involved in epithelial-to-mesenchymal transition (EMT).[10] Recent evidences indicate that ZEB1 could also regulate immune cell functions. Indeed, reciprocally to ZEB2, another member of the ZEB family, ZEB1, is expressed by a variety of immune cells,[11] with immune suppressive functions. In tumor-associated macrophages, ZEB1seems to promote their polarization toward a pro-tumor phenotype[12]; it also acts as a repressor of miR-200, which negatively regulates the expression of the PD-L1 immune checkpoint.[13] As mutated counterparts of normal myeloid cells,[8] AML blasts could adopt ZEB1 expression to modulate the leukemia microenvironment. The expression of ZEB1 has been already reported in leukemia, leading to different and, sometimes, opposite conclusions, being that ZEB1 described as both pro- and anti-leukemogenic.[14–16]

In this study, we functionally explored the impact of ZEB1 in murine leukemia cells seeding the BM microenvironment and confirmed data and clinical relevance in patients with AML.

RESULTS

The median of *ZEB1* expression dichotomizes patients with AML and defines patients with worse OS and peculiar immune features

To define the relevance of ZEB1 in AML, we performed *in silico* analysis on 7 independent cohorts from publicly available datasets (GEO: GSE15434, GSE16015, GSE12417, GSE37642, GSE6891, and GSE161532 and TCGA; see the key resource table and Figure S1A for the principal-component analysis) for a total of 1,325 patients with AML. Patients with AML were subdivided into two groups considering the median value of *ZEB1* expression among patients to bisect *ZEB1*^{high} and *ZEB1*^{low} AML (Figure 1A). To identify the main characteristics of *ZEB1*^{high} and *ZEB1*^{low} AML, we performed a pathway analysis (Figure 1B) pointing out differences in the expression of immune response programs, including inflammatory response, interferon γ (IFNγ) response, and allograft rejection, that were down-regulated in *ZEB1*^{high} patients. On the contrary, *ZEB1*^{high} patients showed an enrichment in MYC, HEME metabolism, interleukin-17A (IL-17A), and transforming growth factor β (TGF-β) pathways. Of note, by combining datasets for a total of 1,298 patients with known OS (GEO: GSE12417, GSE37642, GSE6891, and GSE161532 and The Cancer Genome Atlas [TCGA]), we found shorter OS in *ZEB1*^{high} than *ZEB1*^{low} patients with AML (Figure 1C).

Considering clinical features such as karyotype, French-American-British (FAB) classification, and OS of patients with AML, we observed a significant difference between *ZEB1*^{high} and *ZEB1*^{low} among cytogenetic subgroups (GEO: GSE6891, p = 5.00E−07; TCGA-AML+ Beat AML, p = 5.00E−07) (Figure S1B), with higher and lower percentages of normal karyotype- and core-binding factor-mutated AML (t(8; 21) and inv(16)) in *ZEB1*^{high} versus *ZEB1*^{low} cases, respectively. The different distribution according to FAB classification was also confirmed (GEO: GSE6891, p = 1.00E−07; GEO: GSE37642, p = 4.60E−06; TCGA-AML+ Beat AML, p = 3.00E−07) (Figure S1B), with *ZEB1*^{high} AML being enriched for more undifferentiated leukemia types. The large number of cases in the cohorts of public datasets allowed testing the association between *ZEB1* expression and the AML mutational profile. *ZEB1*^{high} and *ZEB1*^{low} cases showed a similar frequency of *ASXL1*, *DNMT3A*, *IDH1*, *IDH2*, *KRAS/NRAS*, *RUNX1*, *NPM1*, and *FLT3*-ITD mutations but differed for the concomitant presence of *FLT3*-ITD and *NPM1* mutations: 15.8% versus 5.8% in *ZEB1*^{high} versus *ZEB1*^{low}, respectively (Figure S1C). In line with cytogenetic data, *ZEB1*^{high} also included a higher percentage of *TP53*-mutant patients (13.5% versus 3.6% of *ZEB1*^{low}, p = 0.004), while *CEBPA* biallelic mutations were only present in the *ZEB1*^{low} cohort (6.6% versus 0% of *ZEB1*^{high}, p = 0.003) (Figure S1D). The data as a whole suggest that ZEB1

Figure 1. The median of *ZEB1* expression dichotomizes patients with AML and defines patients with peculiar immune features and worse OS

(A) *ZEB1* expression levels in the gene expression profile (GEP) analysis performed combining 7 independent AML cohorts (GEO: GSE15434, GSE16015, GSE12417, GSE37642, GSE6891, and GSE161532 and TCGA) for a total of 1,325 patients with AML (see also Figure S1 and Table S1).

(B) Relevant pathways associated with *ZEB1*^{high} and *ZEB1*^{low} AML blasts in the 7 cohorts.

(C) Kaplan-Meier (KM) curves showing *ZEB1*^{high} and *ZEB1*^{low} patients' overall survival (OS) combining the AML cohorts for which OS data were available (GEO: GSE12417, GSE37642, GSE6891, and GSE161532 and TCGA) for a total of 1,298 patients.

(D) Western blot analysis showing ZEB1 expression in WEHI-3B and C1498 murine AML cell lines. BM-derived mesenchymal stem cells (MSCs) isolated from BALB/c (B/c) mice were used as ZEB1^{+} control. β-Actin was used as internal control.

(E) Stable knockdown of *Zeb1* in C1498 using lentiviral vectors evaluated by western blot and qPCR. β-Actin was used as internal control. See also Figures S2A and S2B.

(F) XTT proliferation assay performed on *Zeb1*-expressing (scramble [Scr]) and -silenced cell lines. Cell proliferation for each time point was calculated as the (absorbance [Abs] at 450 nm – Abs at 670 nm) $t_{24}/t_{48}/t_{72}$)/(Abs at 450 nm – Abs at 670 nm) t_0 × 100. Data represent a pool of 2 independent experiments; n = 12 biological replicates/each experiment.

(G) *In vitro* invasion assay using 24-well Transwell plates (5 μm pore size) coated with 1 mg/mL Matrigel growth factor reduced basement membrane matrix. Five consecutive fields per Transwell were counted (n = 3/each; one-way ANOVA; Kruskal-Wallis [KW] test p = 0.0064).

(H) Volcano plot showing the up-regulated and down-regulated genes in Scr versus silenced cells.

(I) Heatmap of canonical pathway enrichment analysis performed on *Zeb1*-expressing versus -silenced (sh*Zeb1*-seq-C and sh*Zeb1*-seq-D, respectively) cells.

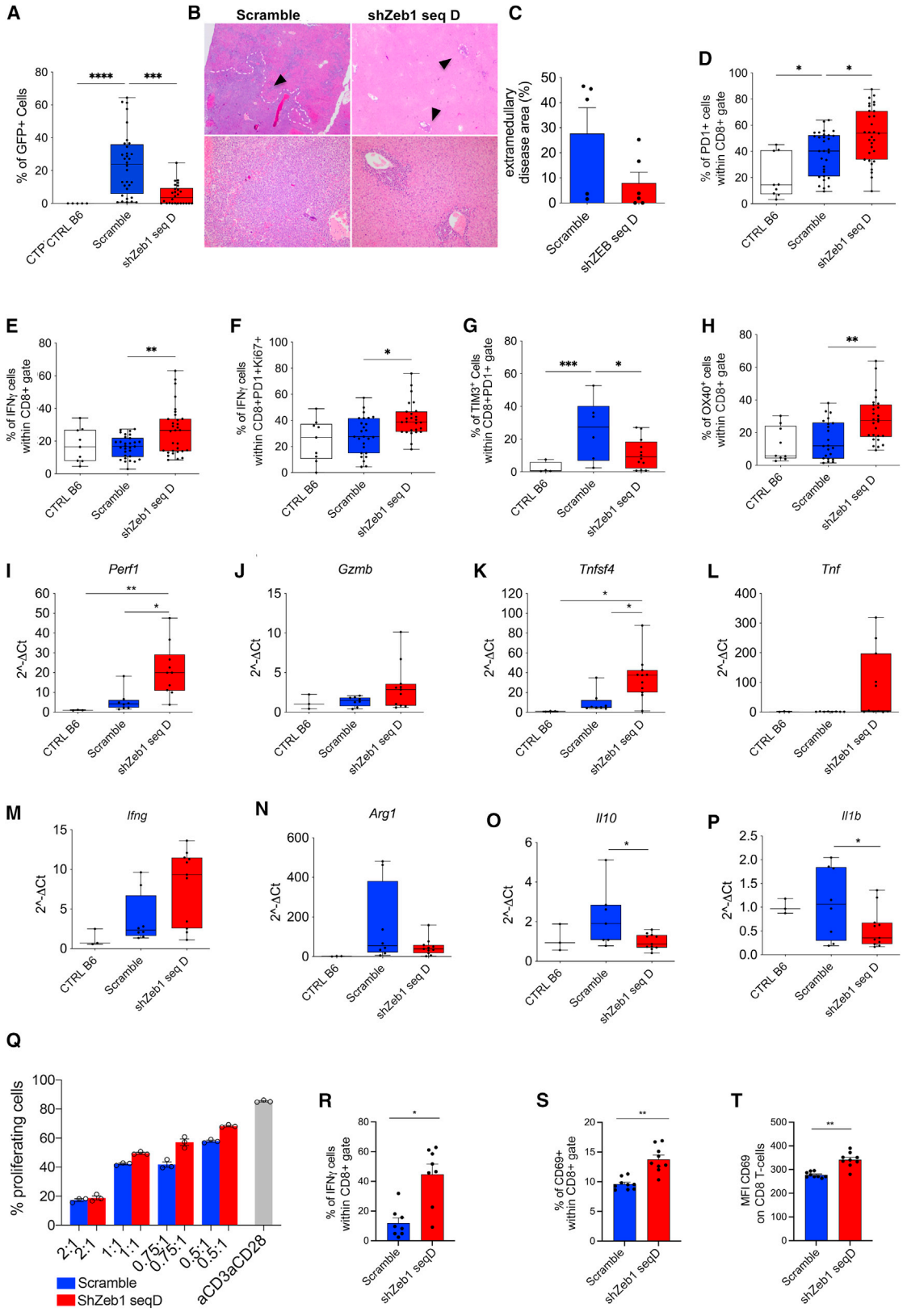

(legend on next page)

might have an adverse impact on leukemia, potentially due to alterations in the immune microenvironment.

Zeb1 gene silencing impairs the invasive ability of leukemic C1498 cells without affecting their proliferation

To model the activity of ZEB1 in the context of leukemia, we started evaluating its expression in two widely used, and well-characterized, AML murine cell lines, C1498 and WEHI-3B cells.[17,18] Western blot (WB) analysis showed high levels of ZEB1 in C1498 cells and its paucity in WEHI-3B cells (Figure 1D). C1498 cells were stably silenced for *Zeb1* using a lentiviral vector also carrying a GFP tag to allow fluorescence-activated cell sorting of infected C1498-GFP$^+$ cells. All target-specific short hairpin RNA (shRNA) significantly decreased *Zeb1* expression compared to scramble transduced control (Figure 1E). In a reverse approach, we tried to overexpress *Zeb1* in WEHI-3B cells. Despite efficient transduction, according to GFP expression and *Zeb1* mRNA expression (Figure S2A), WEHI-3B cells failed to express ZEB1 protein (Figure S2B). A similar result was obtained transducing ZEB1 in human OCI-AML3 cells, in which mRNA, but not ZEB1 protein, was detectable upon gene transduction (data not shown). Hence, we focused on murine and human cell lines endogenously producing ZEB1 and their silenced counterparts because it was unfeasible to force ZEB1 expression in low/negative cells. We first investigated whether *Zeb1* silencing in C1498 cells could negatively impact cell growth or invasiveness. *In vitro* experiments showed that *Zeb1* down-regulation did not significantly affect cell proliferation (Figure 1F) but had some impacts on the C1498 differentiation state, increasing the frequency of C1498 cells positive for the intracellular markers Mac-3, CD115, and CD3[17] (Table S2). Differently, *Zeb1* silencing significantly reduced the invasive properties of C1498 cells (Figure 1G), suggesting a possible role of ZEB1 in regulating the aggressiveness of AML cells. Given the different behavior of *Zeb1*-expressing versus -silenced C1498 cells, we compared their gene expression profiles. Results showed 56 up-regulated and 160 down-regulated genes in control versus sh*Zeb1*-seq-C and 73 up-regulated and 91 down-regulated genes in control versus sh*Zeb1*-seq-D (Figure 1H). Notably, *Zeb1*-expressing cells had higher expression of genes related to Myc and E2F pathways or involved in the mTOR signaling compared to their silenced counterpart (Figure 1I). Also, *Zeb1*-expressing cells had a decreased expression of inflammatory and immune-related pathways, among them tumor necrosis factor (TNF), IFNα, and IFNγ (Figure 1I), confirming the human data and supporting the involvement of ZEB1 in immune regulation.

Impaired BM engraftment of *Zeb1*-silenced AML cells is associated with cytotoxic CD8$^+$ T cell expansion

To better recapitulate the AML microenvironment and to test the immune regulatory activity of ZEB1 *in vivo*, *Zeb1*-expressing (scramble transduced) or -silenced (sh*Zeb1*) C1498 cells were injected orthotopically, intra-bone (i.b.), into the tibia of immunocompetent, syngeneic C57BL/6 mice. A lower frequency of GFP$^+$ leukemic cells was found in the BM of mice injected with sh*Zeb* versus scramble transduced C1498 cells (Figure 2A for sh*Zeb1*-seq-D; Figure S3A sh*Zeb1*-seq-C). This finding was associated with reduced extent of diffuse and nodular blast infiltration of liver parenchyma occurring in silenced versus control

Figure 2. Zeb1 down-regulation was associated with the promotion of a cytotoxic microenvironment

(A) Scr (n = 32) and sh*Zeb1*-seq-D (n = 26) were injected in the tibia of immunocompetent C57BL/6 mice, and the percentage of GFP$^+$ cells within the BM was evaluated with flow cytometry 34 days post-injection. Naive mice (n = 5) were used as controls. Data represent a pool of 3 independent experiments (statistical analysis: one-way ANOVA; for multiple comparison ****p < 0.0001; ***p < 0.001; KW test p < 0.0001).

(B) Representative hematoxylin and eosin staining of liver explanted from Scr-injected and sh*Zeb1*-seq-D-injected mice. 10× and 20× magnifications are shown.

(C) Extramedullary disease area quantification of liver explanted by Scr-injected and sh*Zeb1*-seq-D-injected mice. Data represent the quantification of an individual experiment (n = 5; unpaired t test; p = 0.09).

(D) Frequencies of CD8$^+$PD1$^+$ within the BM of control mice (CTRL B6, naive, n = 9) or mice injected with *Zeb1*-expressing (Scr, n = 31) or -silenced cells (sh*Zeb1*-seq-D, n = 31). Data represent a pool of 3 independent experiments (statistical analysis: one-way ANOVA followed by Tukey's multiple comparison, p = 0.0001; the p values relative to the comparisons Scr versus CTRL or versus shZeb1-seq-D are shown in the figure; *p < 0.05).

(E) Frequencies of CD8$^+$IFNγ^+ within the BM of control mice (CTRL B6, naive, n = 9) or mice injected with *Zeb1*-expressing (Scr, n = 31) or -silenced cells (sh*Zeb1*-seq-D, n = 31). Data represent a pool of 3 independent experiments (statistical analysis: one-way ANOVA followed by Tukey's multiple comparison, p = 0.0004; the p values relative to the comparisons Scr versus shZeb1-seq-D are shown in the figure; **p < 0.01).

(F) Frequencies of IFNγ^+ cells within the gate of CD8$^+$PD1$^+$Ki67$^+$ (CTRL B6, n = 9; Scr, n = 26; sh*Zeb1*-seq-D, n = 26). Data represent a pool of 2 independent experiments (statistical analysis: one-way ANOVA followed by Tukey's multiple comparison, p = 0.0038; the p value relative to the comparisons Scr versus sh*Zeb1*-seq-D is shown in the figure; *p < 0.05).

(G) Frequencies of CD8 exhausted (PD1$^+$TIM3$^+$) cells within the BM of control mice (CTRL B6, naive mice, n = 4) or mice injected with *Zeb1*-expressing (Scr, n = 6) or -silenced cells (sh*Zeb1*-seq-D, n = 12) (statistical analysis: one-way ANOVA followed by Tukey's multiple comparison, p = 0.0178; the p value relative to the comparisons Scr versus CTRL or Zeb D is shown in the figure; *p < 0.05; ***p < 0.001).

(H) Percentage of CD8$^+$OX40$^+$ lymphocytes within the BM of mice (CTRL B6, n = 9; Scr, n = 22; sh*Zeb1*-seq-D, n = 26). Data represent a pool of 2 independent experiments (statistical analysis: one-way ANOVA followed by Tukey's multiple comparison, p = 0.0009; the p value relative to the comparisons Scr versus *shZeb1*-seq-D is shown in the figure; **p < 0.01).

(I–P) mRNA levels of (I) *Perforin1* (*Prf1*) (KW test, p = 0.001; *p < 0.05; **p < 0.01); (J) *Granzyme B* (*Gzmb*) and (K) *Ox40L* (*Tnfsf4*) (KW test, p = 0.002; *p < 0.01); (L) *Tnf*, (M) *Ifng*, and (N) *Arginase 1* (*Arg1*) (KW test, p = 0.0133); (O) *Il10* (KW test, p = 0.0458; *p < 0.05); and (P) *Il1b* (KW test, p = 0.0458; *p < 0.05) and within the BM of mice injected with C1498-expressing (n = 8) or -silenced cells (n = 11). BM of naive mice (n = 3) was used as control.

(Q) Suppression assay performed by culturing irradiated Scr and sh*Zeb1*-seq-D cells with αCD3-αCD28-stimulated proliferation-dye-labeled T cells at different ratios. Proliferation was assessed 48 h afterward. Data represent 1 experiment out of 3 performed (n = 3 biological replicates).

(R) Percentage of IFNγ-expressing CD8 T cells in the co-culture (n = 8 biological replicates/group).

(S and T) Frequency and mean fluorescence intensity (MFI) of CD69 on CD8 T cells (statistical analysis: unpaired t test **p < 0.01; *p < 0.05; n = 9 biological replicates/group). See also Figures S2–S4 for additive data.

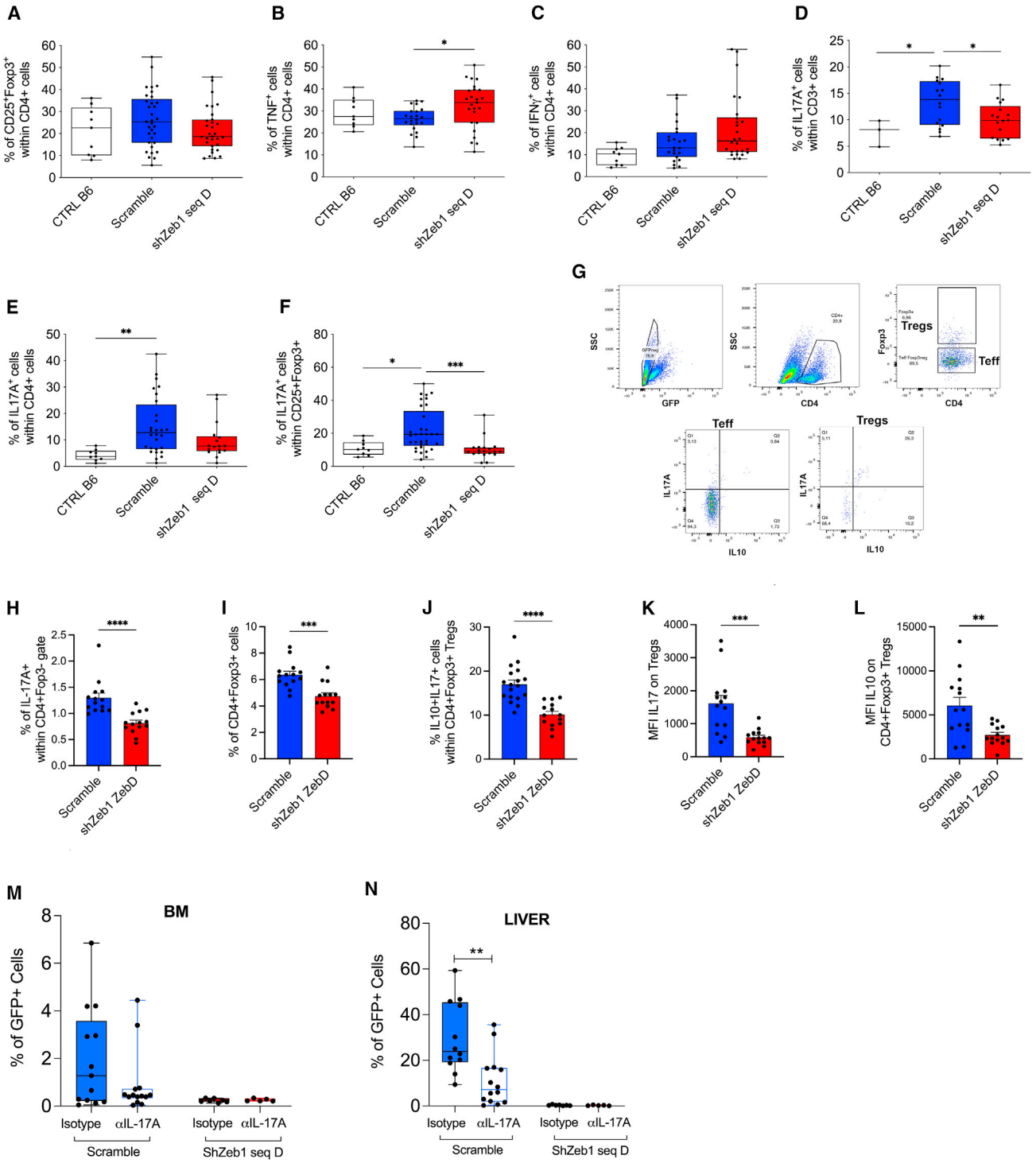

Figure 3. Zeb1 expression is associated with an expansion of lymphocytes producing IL-17A that, in turn, promote AML aggressiveness

(A) Frequency of Treg cells ($CD4^+CD25^+Foxp3^+$) within the BM of control mice (CTRL B6, naive, n = 9) or mice injected with ZEB1-expressing (Scr, n = 33) or -silenced cells (sh*Zeb1*-seq-D, n = 31).

(B and C) Frequency of activated CD4 lymphocytes producing (B) TNF and (C) IFNγ (CTRL B6, naive, n = 9; Scr, n = 22; sh*Zeb1*-seq-D, n = 25) (statistical analysis: KW test, p = 0.0388; for the multiple comparisons: *p < 0.05).

(D–F) Frequency of (D) $IL\text{-}17^+$ $CD3^+$ cells (CTRL B6, naive, n = 3; Scr, n = 16; sh*Zeb1*-seq-D, n = 17) (statistical analysis: KW test, p = 0.0289; for the multiple comparisons: *p < 0.05); (E) $IL\text{-}17^+$ $CD4^+$ cells (CTRL B6, naive, n = 9; Scr, n = 28; sh*Zeb1*-seq-D, n = 16) (statistical analysis: KW test, p = 0.0115; for the multiple

(legend continued on next page)

injected groups (Figure 2B). Notably, the silenced group, exemplified by sh*Zeb1*-seq-D cells, showed leukemic cells mostly confined around blood vessels (Figures 2B and 2C). A reduction in the frequency of C1498 was also observed in the ovary of in mice injected with sh*Zeb1* cells (Figure S3B). Notably, the reduced capacity of sh*Zeb1* cells of extramedullary colonization was better demonstrated in experiments in which AML cells were injected intravenously (i.v.), which is a route of injection favoring liver dissemination.

The relevance of *Zeb*1 in shaping the AML immune microenvironment was investigated by multiparametric flow cytometry analysis performed on BM cells of mice given an intrabone (i.b.) injection of sh*Zeb1*-silenced or *Zeb1*$^+$ C1498 AML cells.

We found increased frequency of CD3$^+$ cells in the BM of mice injected with *Zeb1*-silenced than *Zeb1*$^+$ cells (sh*Zeb1*-seq-C injection in Figure S3C). This increase in T cells was not due to major CD4$^+$ cell increment (sh*Zeb1*-seq-C injection in Figure S3D) but was mainly due to a significant expansion of CD8$^+$ T cells in the BM of mice bearing sh*Zeb1*-seq-D cells versus scramble-treated C1498 cells (Figure S3E) (sh*Zeb1*-seq-C injection in Figure S3F).

Looking at the CD8 subpopulations, we observed a higher frequency of CD8$^+$PD1$^+$ (Figure 2D) and CD8$^+$IFNγ^+ (Figure 2E) T cells in the BM of mice receiving *Zeb1*-silenced than *Zeb1*$^+$ control cells. Since PD1 is expressed on activated CD8 T cells but is also a marker of exhaustion, another marker of exhaustion, such as TIM3, was evaluated along with the ability to produce IFNγ. We found an increased CD8$^+$PD$^-$1$^+$Ki67$^+$IFNγ^+ cell fraction (Figures 2F; Figures S3G and S3H for the sh*Zeb1*-seq-C injection). Concomitantly, the reduction of PD1$^+$TIM3$^+$ cell frequency (Figures 2G; Figure S3H for the sh*Zeb1*-seq-C injection) in the BM of mice injected with *Zeb1*-silenced cells confirms that *Zeb1* down-regulation in leukemic cells unleashes the expansion of activated T cells. Accordingly, the frequency of OX40$^+$CD8$^+$ lymphocytes was higher in BM injected with *Zeb1*-silenced cells than controls (Figure 2H).

The activation of CD8$^+$ T cell in the BM was supported by qPCR analysis performed on total BM cells showing the up-regulation of *Perforin1* (*Prf1*) and *Ox4Ol* (*tnfsf4*) and a trend in increase of *Granzyme B*, *Ifng*, and *Tnf* (Figures 2I–2M) in mice injected with sh*Zeb1*-seq-D compared to controls. This phenotype was paralleled by the decrease of genes encoding for immunosuppressive molecules, including *Arg1*, *Il10*, and *Il1β* (Figures 2N–2P). To further test the direct impact of ZEB1$^+$ C1498 AML cells on CD8 T cell activity, we performed an *in vitro* assay in which αCD3/αCD28-stimulated carboxyfluorescein succinimidyl ester-labeled T cells were cultured with either *Zeb1*-silenced or *Zeb1*$^+$ C1498 cells. Results show that *Zeb1*$^+$ cells suppressed CD8 T cell proliferation if compared to sh*Zeb1*-seq-D-silenced cells (Figure 2Q). On the contrary, the presence of sh*Zeb1*-seq-D cells in the T cell co-culture was associated with an increased expression of activation markers, such as CD69 (both frequency and activation; Figures 2R and 2S), and to an increased production of IFNγ in CD8 T cells (Figure 2T). The same experiment has been done with sh*Zeb1*-seq-C-silenced cells, and results are shown in Figures S3I–S3L.

ZEB1 promotes Th17 development to support liver infiltration of leukemia cells

To further characterize the ZEB1-dependent immunosuppressive effect on the BM microenvironment, we analyzed the CD4$^+$ population in the BM of mice injected with sh*Zeb1*-silenced or scramble transduced C1498 AML cells. Although the overall frequency of CD4 T cells was not different, the fraction of Treg cells was slightly reduced (Figure 3A) in favor of a statistically significant expansion of TNF-producing CD4$^+$ cells (Figure 3B) and a trend toward increase of IFNγ^+CD4$^+$ (Figure 3C) cells in the *Zeb1*-silenced group. Furthermore, we observed an expansion of IL-17$^+$ lymphocytes (Figures 3D and 3E), also including IL-17$^+$ Treg cells (Figure 3F) in the BM of mice injected with *Zeb1*$^+$ parental, in comparison to sh*Zeb1*-seq-D-silenced cells (data relative sh*Zeb1*-seq-C-silenced cells are shown in Figures S3M and S3N). Notably, paralleling *in vivo* findings, *in vitro* co-culture experiments between T cells and C1498 cells showed an induction of Th17 cells when T cells were cultured in the presence of *Zeb1*-competent cells. Notably, these experiments also showed an increased frequency of total Treg cells and of IL-17$^+$IL-10$^+$ Treg cells when *Zeb1*-competent cells were co-cultured with T cells (Figures 3G–3J). In line with this, the expression levels of IL-17 and IL-10 were significantly higher in Treg cells co-cultured with parental C1498 cells (Figures 3K–3L).

To test the relevance of IL-17A production by CD3$^+$, CD4$^+$, and Treg cells on AML cell growth and dissemination *in vivo*, IL-17A-neutralizing or isotype-matching monoclonal antibodies (mAbs) were given every 3 days to mice implanted with *Zeb1*-competent or -silenced cells. In line with early experiments suggestive of a limited effect of IL-17 blockade against C1498 cell engraftment in the BM and a more evident impact against liver engraftment, additional experiments changing the route of AML cell injection from i.b. to i.v. showed significant impaired infiltration of C1498 cells into the liver in the presence of anti-IL-17 Abs in comparison to the isotype control group (Figures 3M and 3N). The almost unchanged engraftment of C1498-GFP cells in BM compared to a strong reduction against liver spreading under treatment with anti-IL-17A-neutralizing Abs

comparisons: **p < 0.01); and (F) Treg cells (CD4$^+$CD25$^+$Foxp3$^+$) producing IL-17A (CTRL B6, naive, n = 9; Scr, n = 32; sh*Zeb1*-seq-D, n = 18) (statistical analysis: KW test, p = 0.0005; for the multiple comparisons: *p < 0.05; ***p < 0.001).

(G–L) *In vitro* induction of Treg cells/Th17 differentiation. Irradiated Scr and sh*Zeb1*-seq-D cells were cultured in the presence of αCD3-αCD28-stimulated T-cells. The differentiation of Treg/Th17 cells was assessed after 72h. (G) Representative gating strategy; (H) frequency of IL-17+ effector T-cells (Foxp3$^-$); (I) frequency of CD4$^+$Foxp3$^+$ Treg cells; (J) frequency of IL-10$^+$IL-17$^+$ Treg cells; (K) MFI of IL-17 on Treg cells; and (L) MFI of IL-10 on Treg cells. Biological replicates: n = 14/group (statistical analysis: Mann-Whitney t test **p < 0.01, ***p < 0.001; ****p < 0.0001).

(M–O) Immunocompetent mice were injected with either C1498 Scr or *Zeb1*-silenced cells (5E+5 cells intravenously [i.v.]) at day 0 and then treated with anti-IL-17 neutralizing antibody or its isotype control (50 μg i.p.) every 3 days. Mice were sacrificed after 30 days, and BM and livers were harvested for fluorescence-activated cell sorting (FACS) analysis. Frequency of GFP$^+$ cells within the (M) BM and (N) liver of mice injected with *Zeb1*-expressing or -silenced cells and treated with isotype control (Scr n = 13; sh*Zeb1*-seq-D n = 7) or αIL-17A (Scr n = 14; sh*Zeb1*-seq-D n = 7) (statistical analysis: Mann-Whitney t test **p < 0.01). See also Figures S2 and S3 for additive data.

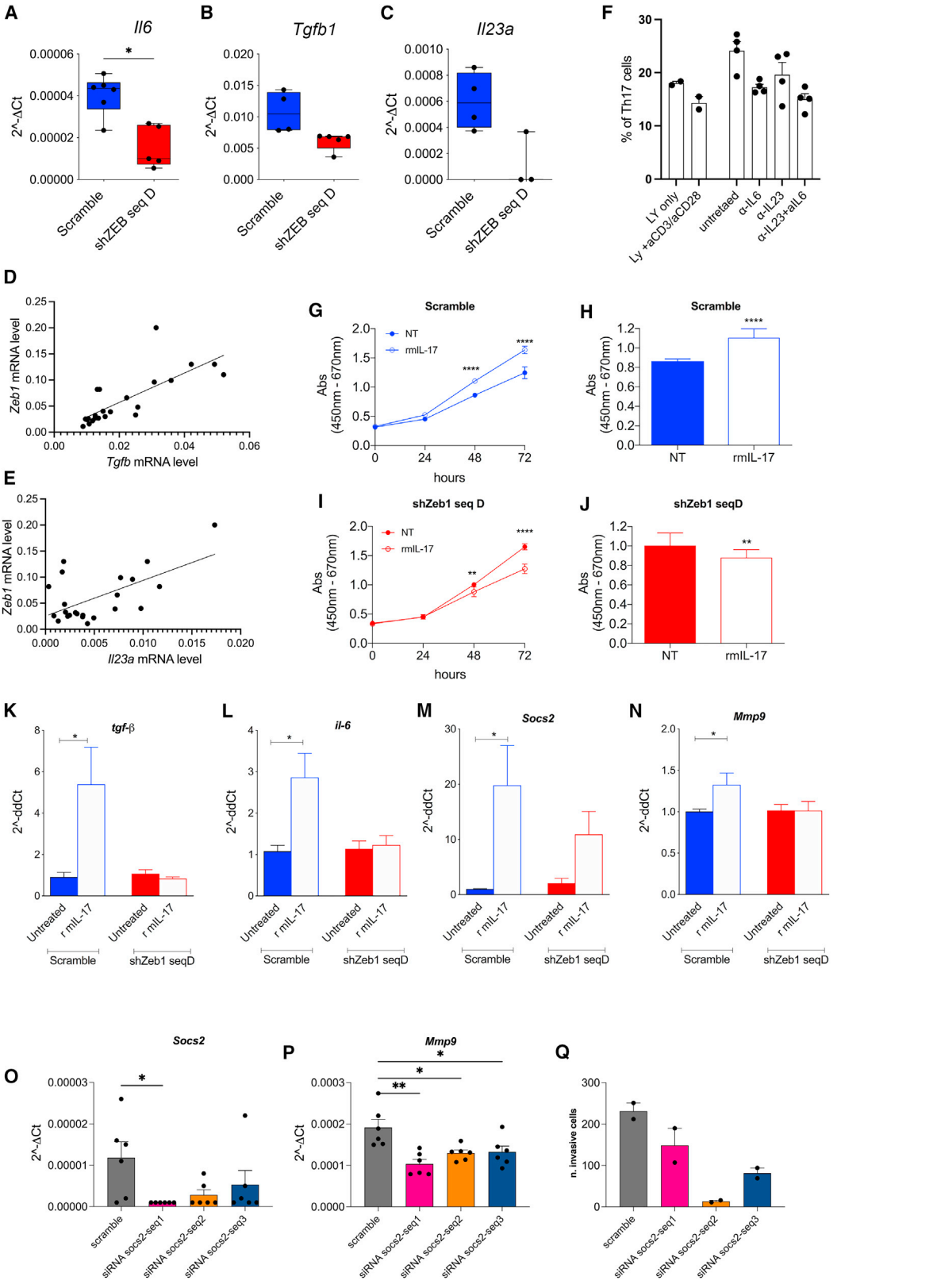

(legend on next page)

suggests a major role of IL-17A in AML dissemination. Notably, the tratement with aIL-17-blocking mAbs did not affect AML cell engraftment in mice injected with sh*Zeb1*-seq-D-/seq-C-silenced cells (Figures 3M and 3N).

ZEB1 supports IL-23, TGF-β, and IL-6 expression toward Th17 development

To provide more insights into the mechanism through which ZEB1 regulates Th17 development, we evaluated the expression of main regulators of Th17 differentiation, *Il6*, *Tgfb1*, and *Il23a*,[19] in *Zeb1*-silenced cells and controls. Results show that *Zeb1* silencing reduced *Il23*, *Il6*, and *Tgfb1* expression in C1498 cells (Figures 4A–4C).

Subcloning C1498 cells at the single-cell level revealed a direct correlation between the *Zeb1* mRNA level and the mRNA levels of *Tgfb1* ($r = 0.7653$; $p < 0.0001$; Figure 4D) and *Il23*a ($r = 0.60$; $p = 0.0023$; Figure 4E) but not of *Il6* ($r = -0.21$), suggesting that Tgfb1 and Il23a gene could be direct targets of ZEB1 activity, whereas IL-6, which is down-regulated in silenced cells, might be an indirect consequence of the above regulation, albeit functionally relevant. Indeed, *in vitro* co-culture experiments between T cells and C1498 cells showed a reduction in Th17 development in the presence of mAbs blocking IL-6 or IL-6 plus IL-23 (Figure 4F).

To better understand how IL-17A might promote AML cell dissemination in relation to ZEB1 expression, *Zeb1*-silenced and *Zeb1*$^+$ C1498 cells were stimulated with recombinant mouse (rm) IL-17 and tested for cell proliferation. Interestingly, rmIL-17 significantly increased the proliferation of *Zeb1*$^+$ cells (Figures 4G and 4H) but not of *Zeb1*-silenced cells (Figures 4I and 4J), suggesting in some way the existence of a relationship between ZEB1 and the capacity of responding to rIL-17, independently from the IL-17R, which is expressed equally in silenced and parental cells (Figure S4A). In line with this, we found a direct correlation between the rate of proliferation in the presence of IL-17 and *Zeb1* mRNA level in C1598 clones ($r = 0.455$; $p = 0.0291$). In parental C1498 cells, rmIL-17 treatment increased the expression of *Tgfb1* and *Il6* but also of *Socs2* and *mmp9* (Figures 4K–4N), which are relevant marker of AML aggressiveness[20,21] directly associated with blast invasion capacity.[22]

To understand the significance of SOCS2 up-regulation in AML cells, C1498 cells were transiently silenced for *Socs2.* In this experiment, we used 1 scramble and 3 target-specific sequences. We show that *Socs2* inhibition reduced *mmp9* expression in C1498 cells and that such a phenotype was associated witha reduced invasive capacity of C1498 cells (Figures 4O–4Q).

To corroborate mouse data in the human setting, we initially investigated ZEB1 expression in a panel of 6 different leukemic cell lines. Among them, only the K562 cells were found to express ZEB1 along with SOCS2 (Figure 5A), allowing the generation of its *ZEB1*-silenced counterpart that proved to be also down-modulated for SOCS2 in both WB and qPCR analyses (Figures 5B–5D) with no impact on cell differentiation status (Figures S4B and S4C). Notably, the *ZEB1*-silenced variant also showed reduced expression of *IL23* and *TGFB1* (Figures 5E and 5F).[23] Furthermore, K562 cell stimulation with rhIL-17 confirmed the induction of *SOCS2*, *MMP9*, and *IL6* (Figures 5G–5I).

Remarkably, the relevance of SOCS2 for ZEB1$^+$ AML was further confirmed in human AML showing the increased expression of *SOCS2* in ZEB1^{high} patients (Figure 5J) in 7 merged independent cohorts from publicly available datasets (GEO: GSE15434, GSE16015, GSE12417, GSE37642, GSE6891, and GSE161532 and TCGA) included in Figure 1.

ChIP-qPCR experiments show that IL-17 sustains the binding of ZEB1 to IL-23, TGF-β1, and SOCS2 promoters and enhancers

To verify that molecules whose expression is affected by ZEB1 depletion are direct targets of this EMT regulator, we interrogate ENCODE web source to prioritize their candidate *cis*-regulatory elements (cCREs), including active promoters and enhancers, and repressed chromatin, inferred by H3K4me1, H3K4me3, H3K27ac, and H3K27me3 chromatin immunoprecipitation sequencing (ChIP-seq) peaks in K562 cells. ENCODE ZEB1 ChIP-seq was available for the GM12878 lymphoma cell line. DNA sequences mapping at the potential cCREs were scrutinized for putative consecutive E-box-based binding sites (CANNTR-containing sequences) for ZEB1[24] through JASPAR, and primers encompassing these regions were designed to perform ChIP-qPCR in control and rIL-17-stimulated K562 cells. By this

Figure 4. IL-17A stimulation promotes the expression of genes associated with leukemic cell aggressiveness

(A) Semi-quantitative qPCR analysis for *Il6,* (statistical analysis: t test; *$p < 0.05$; n = 6/Scr; n = 5 *shZeb1*-seq-D).

(B) qPCR analysis for *Tgfb1* (n = 4/Scr; n = 5 *shZeb1*-seq-D).

(C) qPCR analysis for *Il23a* (n = 4/Scr; n = 3 *shZeb1*-seq-D).

(D and E) C1498 cells were cloned to generate different subclones with variable *Zeb1* expression. For every clone, we evaluated *Zeb1*, *Tgfb*, and *Il23* mRNA levels. The graph in (D) shows the direct correlation between *Zeb1* and *Tgfβ* mRNA levels ($r = 0.76$; $p < 0.0001$); (E) shows the direct correlation between *Zeb1* and *Il23* mRNA levels ($r = 0.60$; $p < 0.0023$).

(F) Frequency of Th17 cells from experiments in which C1498 cells were co-cultured with αCD3/αCD28-stimulated T cells in the presence of mAbs blocking IL-6 (10 μg/mL) and IL-23 (10 μg/mL) (n = 4/experimental group).

(G–J) Cell proliferation of C1498-expressing (Scr) (G and H) or -silenced (sh*Zeb1*-seq-D) (I and J) cells upon IL-17A stimulation (50 ng/mL) assessed by tetrazolium salt XTT assay after 24, 48, and 72 h. Cell proliferation for each time point was calculated as the (Abs at 450 nm – Abs at 670 nm). Bar plots show the proliferation at 48 h. Data represent a pool of 2 experiments; n = 12/group (statistical analysis: two-way ANOVA; multiple comparison test: **$p < 0.01$; ****$p < 0.0001$).

(K–N) qPCR showing the induction of *Tgfβ* (K, n = 5), *Il6* (L; n = 8), *Socs2* (M, n = 7), and *Mmp9* (N, n = 7) upon stimulation (7 days) with IL-17A 50 ng/mL in Zeb1-expressing cells (statistical analysis: paired t test; *$p < 0.05$).

(O) qPCR levels of *Socs2* after 48 h transient silencing performed on C1498 parental cells (n = 6/group; statistical analysis: one-way ANOVA *$p < 0.05$).

(P) *Mmp9* expression levels in *Socs2*-silenced cells (n = 6/group; statistical analysis: one-way ANOVA *$p < 0.05$; **$p < 0.01$).

(Q) *In vitro* invasion assay performed on C1498 silenced for *Socs2* using 24-well Transwell plates (5 μm pore size) coated with 1 mg/mL Matrigel growth factor reduced basement membrane matrix. Two experiments performed with three consecutive fields per Transwell counted (the points represent the media of each experiment). See also Figure S4 for additional data.

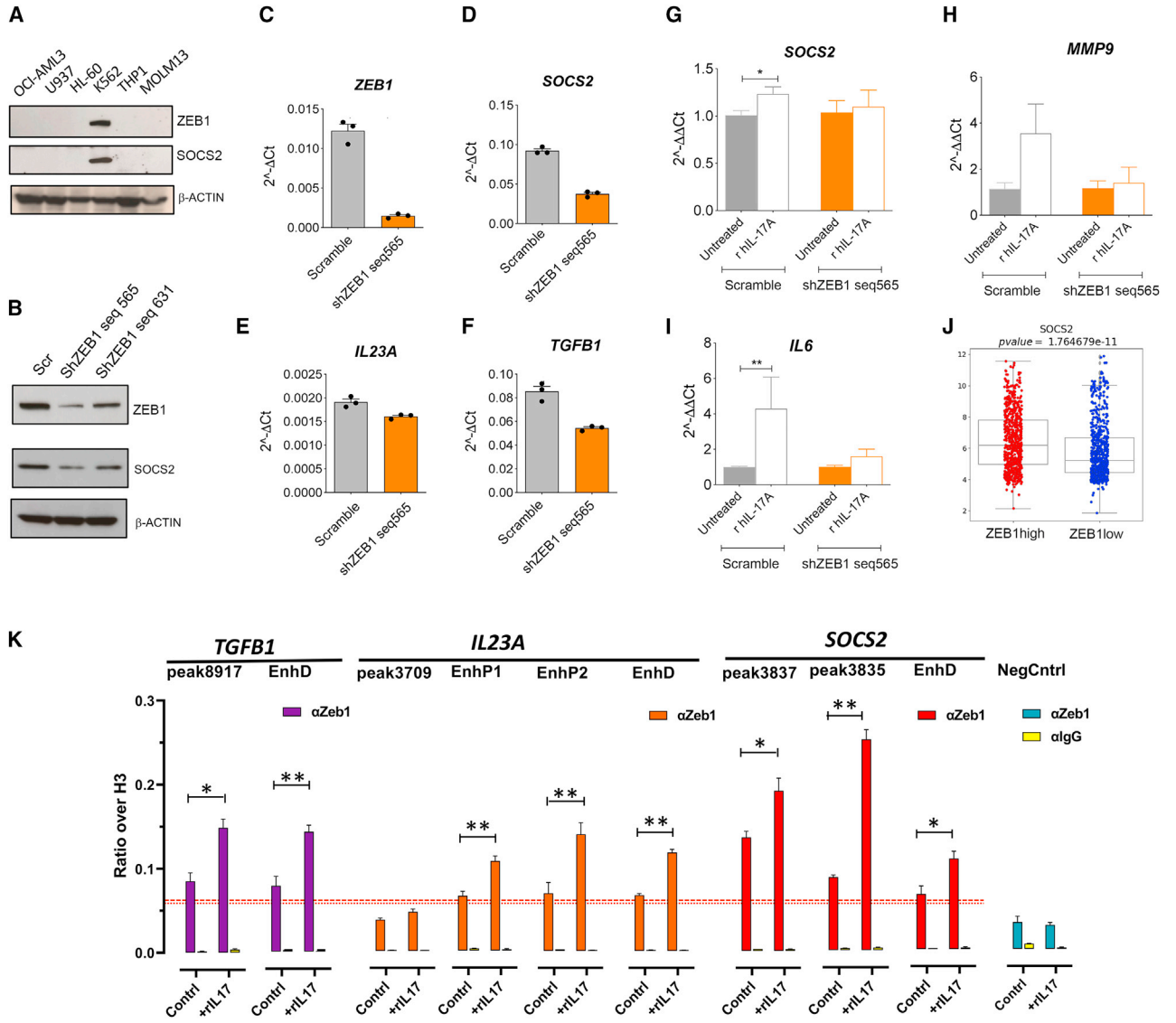

Figure 5. IL-17 favors ZEB1 binding to IL-23, Tgfb, and SOCS2 promoters

(A) *ZEB1* expression in a panel of 6 different leukemic cell lines evaluated by western blot.

(B) Stable knockdown of *ZEB1* in K562 using lentiviral vectors evaluated by western blot. β-Actin was used as internal control.

(C–F) Semi-quantitative qPCR analysis for (C) *ZEB1*, (D) *SOCS2*, (E) *IL23A*, and (F) *TGF* in *K562* cells silenced for *ZEB1* and relative Scr control.

(G–I) Semi-quantitative qPCR showing the induction of (G) *SOCS2* (*p < 0.05), (H) *MMP9*, and (I) *IL6* (**p < 0.01) upon stimulation (7 days) with IL-17A 50 ng/mL in ZEB1-expressing cells (n = 3 biological replicates/group).

(J) SOCS2 expression level in the AML dataset.

(K) Zeb1 enrichment at cCREs of *TGFB1*, *IL23A*, and SOCS2 genes. Calling of Zeb1 binding and permissive chromatin marks at cCREs for Zeb1 occupancy was addressed by the ENCODE Project (see Figures S5–S7) and verified by ChIP-qPCR in K562 cells. By setting the level of biological significance at 2-fold the value of background (NegCntrl: dashed red line for control cells; dotted red line for rIL-17-stimulated cells), three Zeb1 binding sites were confirmed at promoters of *SOCS2* (peaks 3835/3837) and *TGFB1* (peak 8917) in control cells ($p < 0.005$). Most of the cCREs showed improved ZEB1 occupancy with significance following rIL-17 stimulation (statistical analysis: paired t test between control (Contrl) and treated cells; unpaired t test between each cCREs and corresponding NegCntrl; *$p < 0.05$; **$p < 0.01$). See also Figures S5–S7 for additive data.

approach, to corroborate gene expression data, we assayed ZEB1 direct binding to cCREs within 50 kb of TGF-β1, IL-23A, and SOCS2 transcription start sites, as well as an unrelated negative control locus (centered on the rs667515 SNP mapping at chr11q13.3) devoid of clustered E-box motifs, and of H3K4me3/H3K27ac permissive chromatin marks. As shown in Figures 5K and S5A–S5C, the ZEB1 transcription factor significantly binds to each locus analyzed, as opposed to immunoglobulin G^{-} controls, which might indicate its widespread distribution in the genome due to its affinity to degenerate ZEB1 motifs and to additional binding sites in cooperation with co-factors.[25] However, most of the cCREs assayed show an enrichment of ZEB1

occupancy as compared to the unrelated control locus. Notably, cells stimulated by rIL-17 demonstrated the most up-regulation of ZEB1 binding to these loci, which parallels an increase of permissive chromatin marks at certain cCREs (Figures 5K and S5–S7). This finding appears to underpin ZEB1-dependent up-regulation of these target genes by IL-17.

Underscoring the Th17-ZEB1 axis in human AML reveals an association between ZEB1 and AML relapse

To further challenge the association between ZEB1 expression in leukemic blasts and Th17, we performed a double immunofluorescence (IF) staining on archival BM biopsies from 26 patients with AML divided into ZEB1^{high} and ZEB1^{low} according to the median number of ZEB1^{+} nuclei, which ranged from 0.5% up to 60% (Figure 6A). Results show a higher number of CD3^{+}IL-17^{+} cells in ZEB1^{high} than ZEB1^{low} AML cases (Figures 6B and 6C), with a positive correlation between ZEB1 levels and the number of CD3^{+}IL-17A^{+} cells (Figure 6D). Accordingly, a gene signature able to identify Th17 cells in TSGA AML cohorts using the GEPIA2 tool revealed an association with poor outcome in terms of OS (Figure 6E) in patients enriched for this signature.

Given the known activities of ZEB1 in drug resistance,[26] we investigated its possible role in AML relapse. To this end, we performed *in silico* studies using gene expression profiling analysis on paired AML blasts obtained at diagnosis and relapse (GEO: GSE66525).[27] We found a remarkable increase of ZEB1 expression in relapsed samples compared to the baseline at diagnosis (Figures 7A and 7B), along with increased expression of SOCS2 (Figure 7C). Concordantly, in these same patients, the higher level of ZEB1 in relapsed patients was associated with the enrichment of the Th17 pathway (Figure 7E). Moreover, by investigating the differentially expressed hallmarks at relapse compared to at diagnosis, we found up-regulation of MYC targets and ultra-violet (UV) response and a down-regulation of inflammatory response, allograft rejection, and IFNγ response (Figure 7E), all pathways related to ZEB1^{+} blasts. This finding supports the hypothesis that relapsed AML is enriched in ZEB1^{+} blasts that maintain the ZEB1-driven Th17 skewing.

Association between ZEB1 and chemoresistance

To test the relevance of ZEB1 in chemotherapy response, we went back to immune-competent mouse models and treated AML-bearing mice with cytarabine (AraC) *in vivo*. To this end, C57BL/6 mice were injected i.b. with scrabble C1498 cells or *Zeb1*-silenced clones. Starting 9 days after leukemia cell injection, mice were treated with AraC (50 mg/kg) (Figure 7F). Results show that AraC treatment was more efficient in reducing the AML cell engraftment of *Zeb-1*-silenced than *Zeb-1*-proficient leukemia cells. Indeed, mice injected with *Zeb-1*-silenced cells showed increased OS, evaluated using humane endpoint criteria (Figure 7G), paralleled by a reduced frequency of leukemia cells in BM, liver, and ovary when euthanized (Figures 7H–7J).

DISCUSSION

Nowadays, it is widely accepted that AML cells can influence the BM microenvironment to their own advantage such as to create a peculiar niche that supports their survival, resistance to therapy, and immune evasion. Nevertheless, beside IFNγ, no other molecular drivers active in molding the BM immune microenvironment under AML influence have been characterized in depth.[3,28] Here, we demonstrate a previously unknown activity of the EMT regulator ZEB1 in shaping the BM immune microenvironment, when expressed by leukemic blasts, sustaining AML progression. Our data indicate that ZEB1 directly orchestrates a T cell immune microenvironment favoring Treg cells and Th17 cell expansion. IL-17, in turns, promotes proliferation and invasion of ZEB1^{+} cells.

Previous studies performed on AML characterized by the *MLL-AF9* fusion gene showed ZEB1 expression associated with aggressive LT-HSC-derived AML and with reduced OS. Regarding the potential oncogenic activity of ZEB1 in AML,[16,14,15] discordant pieces of evidence have been published. Almotiri and colleagues postulated that ZEB1 acts as a transcriptional regulator of hematopoiesis and that its expression is required to suppress leukemic potential in AML models.[29] These data might fit with our failure in over-expressing ZEB1 protein despite efficient gene transduction and mRNA expression in both mouse and human cell lines that endogenously are low/negative for ZEB1. Differently, the possibility of silencing ZEB1 where it is spontaneously expressed suggests a cell-dependent protein dosage limitation. Our analysis of ZEB1 expression and distribution in larger datasets, including those evaluated by Almotiri, revealed that when patients were categorized into two groups based on the median level of ZEB1 expression, it is possible to identify two distinct groups, *ZEB1*^{high} and *ZEB1*^{low}, each with unique immunological and molecular characteristics. At the molecular level, *ZEB1*^{high} patients with AML showed increased expression of pathways related to MYC, IL-17, SOCS2, TGF-β, and HEME metabolism and down-modulation of inflammatory pathways, along with a negative association with OS. However, it is important to emphasize that, when evaluated at the RNA level in datasets, the expression of ZEB1 can be lower than in normal BM that is rich in ZEB1^{+} cells (granulocytes, T cells). This is in line with the immunohistochemistry (IHC) analysis showing that ZEB1 staining does not always encompass the entire blast population. What is to be underscored is that, although underrepresented, ZEB1^{+} blasts with their distinctive characteristics could have highly significant functional relevance, for example being more refractory to chemotherapy treatment, as shown in a preclinical study performed by treating C1498-bearing mice with AraC. This is in line with the concept that although clonal evolution is associated with AML resistance after chemotherapy or hematopoietic stem cell transplantation, leukemia cells initially present at disease onset may also have features of intrinsic resistance associated with immune regulatory functions and be responsible for relapse.

Our IHC/IF analyses and *in silico* data from GEO: GSE66525 indicate that the presence of ZEB1^{+} blasts is associated with a unique immune environment rich in Th17 cells and Treg cells. Extending the analysis of ZEB1 to larger cohorts of patients will help define whether ZEB1 could be endowed with a prognostic role.

If the prognostic role of ZEB1 is not known, then there are already data demonstrating the prognostic relevance of the associated immune microenvironment. Musuraca and

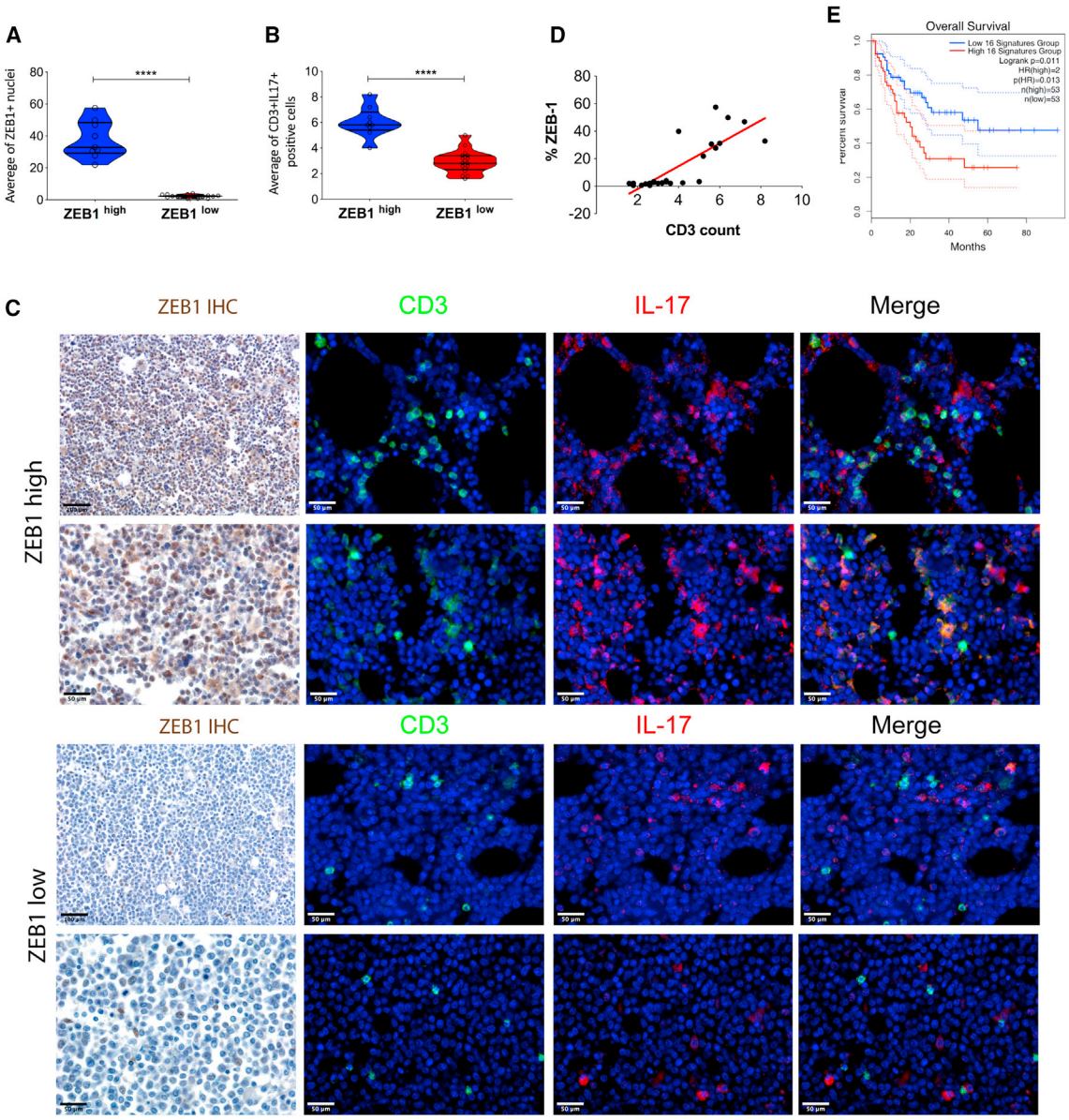

Figure 6. ZEB1^{high} levels in patients with AML positively correlate with the expansion of IL-17^{+} CD3 cells

(A) ZEB1 quantitative analysis of immunohistochemical staining performed using the Image Analysis software provided by Leica ("nuclear hub" tool) (statistical analysis: Mann-Whitney t test ****$p < 0.0001$).

(B) Quantification of CD3^{+}IL-17^{+} cells within the BM of ZEB1^{high} (n = 9) and ZEB1^{low} (n = 17) patients with AML (statistical analysis: Mann-Whitney t test ****$p < 0.0001$).

(C) Representative immunohistochemical staining for ZEB1 and immunofluorescence for CD3^{+}IL-17A^{+} evaluation (CD3 in green and IL-17A in red) performed on 26 archival BM biopsies of patients with AML (University of Palermo cohort). Original magnifications, ×200 and ×400. Scale bars, 50 and 100 μm.

(D) Positive correlation between ZEB1^{+} cells and CD3^{+}IL-17A^{+} infiltrate (statistical analysis: Pearson's correlation; $r = 0.6265$; $p < 0.0001$).

(E) OS of patients with AML (TCGA) with high and low Th17 infiltration. 16 genes (*CXCL3*, *IL22*, *IL3*, *CCL4*, *GZMB*, *LRMP*, *CCL5*, *CASP1*, *CSF2*, *CCL3*, *TBX21*, *ICOS*, *IL7R*, *STAT4*, *LGALS3*, and *LAG3*) were used to define specific cell populations.

colleagues described a population of IL-17/IL-10-secreting immune suppressive Th17 cells that could identify patients with AML with a higher risk of severe infections and relapse.[30] Furthermore, SOCS2, which is induced in leukemic blasts upon rIL-17 treatment, is a well-known AML prognostic factor and a molecule directly involved in controlling leukemia aggressiveness.[20,31]

In the present study, we demonstrate that IL-17 could be a potential chromatin regulator able to enhance the binding of ZEB1 to target promoters, providing a sort of feedback loop that

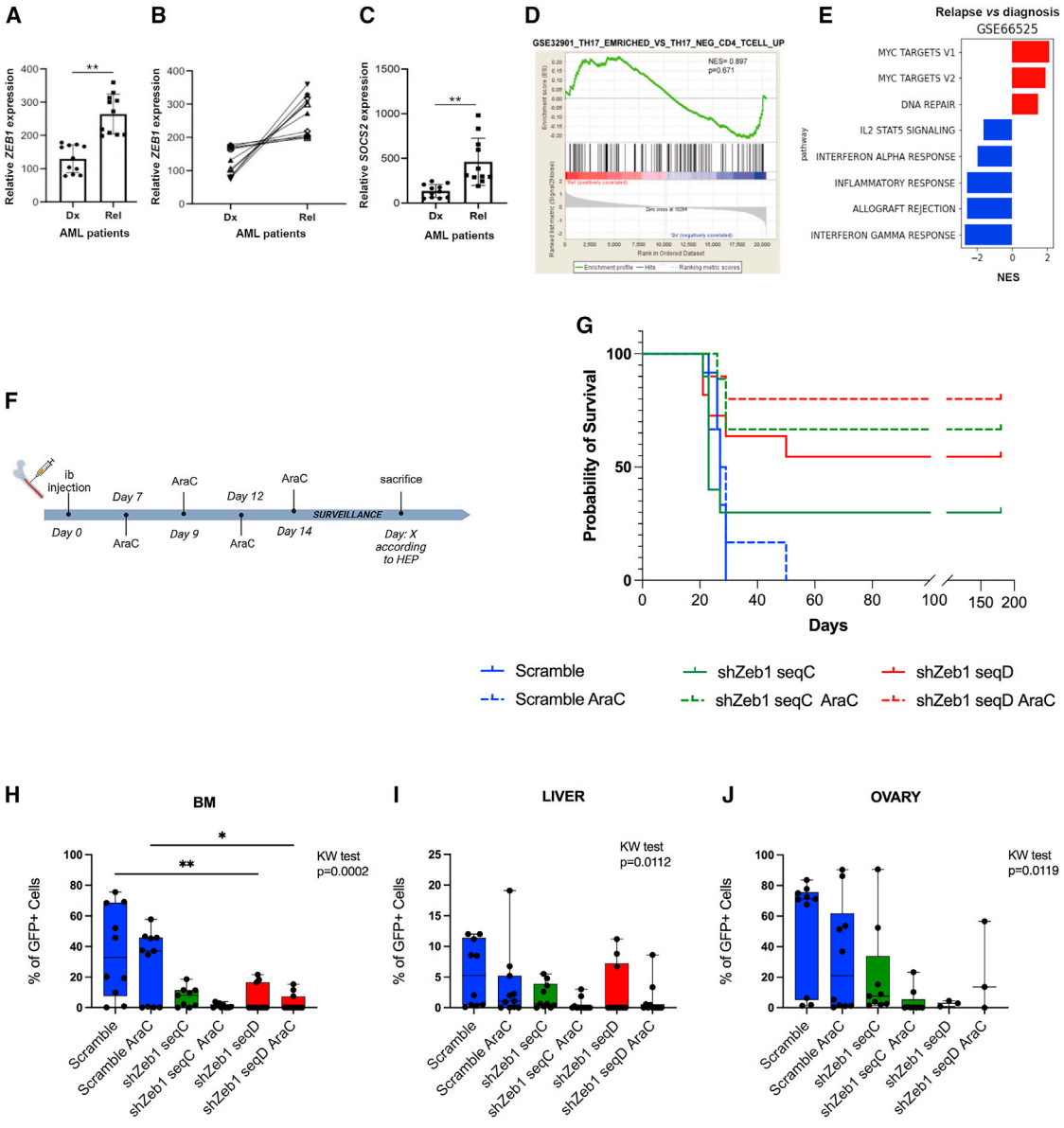

Figure 7. Relevance of Th17-ZEB1 axis in AML relapse

(A and B) *ZEB1* expression levels in the in 11 patients with AML (GEO: GSE66525) (A) also matching each patient at diagnosis (Dx) and relapse (Rel) (B).

(C) Expression levels of *SOCS2* at Dx and Rel in the same dataset.

(D) IL-17 enrichment pathway at Rel versus at Dx.

(E) Hallmark pathways enriched or down-regulated in relapsed patients compared to patients at Dx.

(F) Schematic representation of the experiment. Mice were injected i.b. with the different cell lines and treated with cytarabine (AraC) starting at 7 days after cell injection.

(G) KM survival analysis in mice injected i.b. with Scr (n = 12 untreated versus 12 treated with AraC), sh*Zeb1*-seq-C (n = 10 untreated versus 9 treated with AraC), and seq-D-silenced cells (n = 11 untreated versus 10 treated with AraC). KM was obtained according to human endpoints (HEPs) (statistical analysis: log-rank [Mantel-Cox]; p = 0.0006).

(H–J) Frequency of leukemia cells in BM, liver, and ovary at sacrifice (statistical analysis: KW test, multiple comparison test; *p < 0.05; **p < 0.01).

causes a different gene expression not sustained by underlining mutations (called "epigenetic").

We also show that IL-17 promotes invasion and proliferation of ZEB1^{+} cells only, despite both *Zeb1*-silenced and parental cells having the same level of IL-17R expression. Our ChIP-qPCR analysis, along with data from the ENCODE Project, supported the direct binding of ZEB1 to *SOCS2*, *TGFB1*, and *IL23A* regulatory regions. ZEB1 binding to the cCRE appears to regulate expression of rIL-17 downstream targets through activation of specific candidate regulatory regions.

It remains to be understood why IL-17 exerted some anti-proliferative activity on *Zeb-1*− cells. An anti-proliferative activity of IL-17 has been described only in adult T cell leukemia, where the activation of a RORC/IL-17 pathway had a negative impact on clonality and proliferation.[32] Despite the in-depth and detailed phenotypic characterization of C1498 cells that demonstrated *in vitro* and *in vivo* the myeloid differentiation,[17] some leukemic cells express T cell markers. These cells are present in higher frequency in Zeb1-silenced cells. Therefore, it is possible that the negative effect of IL-17 on proliferation could be ascribed to the effect of IL-17 in this fraction of leukemic cells.

Although there has been advancement in understanding the disease and its treatment strategies, there is a pressing requirement to unravel the fundamental factors associated with AML cases that have a high likelihood of progression and recurrence. This comprehension is vital for the development of novel diagnostic pathways and treatment methods aimed at improving patient outcome. Despite the improvements in the treatment, relapse still represents a common scenario in AML, occurring in 40%–50% of younger and the great majority of elderly patients.[33] We suggest that ZEB1 could be a candidate predictive marker to be targeted using specific approaches.

Finally, our findings, linking ZEB1 to AML immune suppression, are mirrored in solid tumors where EMT factors contribute to immune evasion[34–36] and highlight the need to further investigate the molecular mechanisms by which tumor-intrinsic EMT-related pathways affect the microenvironment.

Limitations of the study

The study is constrained by its emphasis on mechanistic aspects, particularly generated on cell lines instead of primary AML samples. Nevertheless, it is worth mentioning that the relationship between Th17 cells and ZEB1 has been observed in AML patient biopsies despite this limitation.

STAR★METHODS

Detailed methods are provided in the online version of this paper and include the following:

- KEY RESOURCES TABLE
- RESOURCE AVAILABILITY
  - Lead contact
  - Materials availability
  - Data and code availability
- EXPERIMENTAL MODEL AND STUDY PARTICIPANT DETAIL
  - Cell lines
  - Animal models
  - Patients
- METHOD DETAILS
  - Flow cytometry analysis
  - Quantitative immunolocalization analyses
  - Extramedullary disease evaluation
  - Immunoblotting
  - Invasion assay
  - Proliferation assay
  - *In vitro* suppression assay
  - Human transcriptomic data analysis
  - ChIP-qPCR
  - Stable gene-silencing
  - Transient gene-silencing
  - Total RNA extraction, reverse transcription, and quantitative polymerase chain reaction (qPCR)
  - Gene expression profile of mouse cell lines
- QUANTIFICATION AND STATISTICAL ANALYSIS

SUPPLEMENTAL INFORMATION

Supplemental information can be found online at https://doi.org/10.1016/j.celrep.2024.113794.

ACKNOWLEDGMENTS

We thank Dr. Pagani M., Dr. Della Chiara G., and Dr. Bason R. for technical assistance with ChIP-qPCR experiments. The authors also thank Ester Grande for providing administrative support. We thank HOVON for sharing data relative to the AML cohort included in GEO: GSE6891. The research was supported by Fondazione AIRC per la Ricerca sul Cancro (IG22204 to S.S.) and the Italian Ministry of Health: Ricerca Corrente Funds.

AUTHOR CONTRIBUTIONS

Conceptualization, B.B. and S.S.; methodology, C.C. and D.L.; formal analysis, G.S., A.P., and E.F.; investigation, B.B., V.C., A.F., A.M.K., A.G., L.B., P.P., M.C., M.B., G.C., and C.T.; resources, M.C., J.S., A.T., M.P., F.C., and A.C.; writing – original draft, B.B., M.P.C., and S.S.; writing – review & editing, A.C., N.B., M.P.C., and S.S.; visualization, B.B. and S.S.; supervision, M.P.C. and S.S.; funding acquisition, S.S.

DECLARATION OF INTERESTS

The authors declare no competing interests.

Received: March 21, 2023
Revised: November 7, 2023
Accepted: January 30, 2024
Published: February 15, 2024

REFERENCES

1. Lamble, A.J., Kosaka, Y., Laderas, T., Maffit, A., Kaempf, A., Brady, L.K., Wang, W., Long, N., Saultz, J.N., Mori, M., et al. (2020). Reversible suppression of T cell function in the bone marrow microenvironment of acute myeloid leukemia. Proc. Natl. Acad. Sci. USA *117*, 14331–14341. https://doi.org/10.1073/pnas.1916206117.
2. Davidson-Moncada, J., Viboch, E., Church, S.E., Warren, S.E., and Rutella, S. (2018). Dissecting the Immune Landscape of Acute Myeloid Leukemia. Biomedicines *6*, 110. https://doi.org/10.3390/biomedicines6040110.
3. Vadakekolathu, J., Minden, M.D., Hood, T., Church, S.E., Reeder, S., Altmann, H., Sullivan, A.H., Viboch, E.J., Patel, T., Ibrahimova, N., et al. (2020). Immune landscapes predict chemotherapy resistance and immunotherapy response in acute myeloid leukemia. Sci. Transl. Med. *12*, eaaz0463. https://doi.org/10.1126/scitranslmed.aaz0463.
4. Tettamanti, S., Pievani, A., Biondi, A., Dotti, G., and Serafini, M. (2022). Catch me if you can: how AML and its niche escape immunotherapy. Leukemia *36*, 13–22. https://doi.org/10.1038/s41375-021-01350-x.
5. Méndez-Ferrer, S., Bonnet, D., Steensma, D.P., Hasserjian, R.P., Ghobrial, I.M., Gribben, J.G., Andreeff, M., and Krause, D.S. (2020). Bone marrow niches in haematological malignancies. Nat. Rev. Cancer *20*, 285–298. https://doi.org/10.1038/s41568-020-0245-2.

6. Han, Y., Ye, A., Bi, L., Wu, J., Yu, K., and Zhang, S. (2014). Th17 cells and interleukin-17 increase with poor prognosis in patients with acute myeloid leukemia. Cancer Sci. *105*, 933–942. https://doi.org/10.1111/cas.12459.

7. Li, Z., Philip, M., and Ferrell, P.B. (2020). Alterations of T-cell-mediated immunity in acute myeloid leukemia. Oncogene *39*, 3611–3619. https://doi.org/10.1038/s41388-020-1239-y.

8. Mussai, F., Wheat, R., Sarrou, E., Booth, S., Stavrou, V., Fultang, L., Perry, T., Kearns, P., Cheng, P., Keeshan, K., et al. (2019). Targeting the arginine metabolic brake enhances immunotherapy for leukaemia. Int. J. Cancer *145*, 2201–2208. https://doi.org/10.1002/ijc.32028.

9. Curti, A., Salvestrini, V., Aluigi, M., Trabanelli, S., Ottaviani, E., Durelli, I., Horenstein, A.L., Fiore, F., Massaia, M., Piccioli, M., et al. (2007). Modulation of tryptophan catabolism by acute myeloid leukemia cells acts as a general mechanism of immune tolerance via the induction of T regulatory cells. Blood *110*, 1345–405a. https://doi.org/10.1182/blood.V110.11.1345.1345.

10. Caramel, J., Ligier, M., and Puisieux, A. (2018). Pleiotropic Roles for ZEB1 in Cancer. Cancer Res. *78*, 30–35. https://doi.org/10.1158/0008-5472.CAN-17-2476.

11. Scott, C.L., and Omilusik, K.D. (2019). ZEBs: Novel Players in Immune Cell Development and Function. Trends Immunol. *40*, 431–446. https://doi.org/10.1016/j.it.2019.03.001.

12. Cortés, M., Sanchez-Moral, L., de Barrios, O., Fernández-Aceñero, M.J., Martínez-Campanario, M.C., Esteve-Codina, A., Darling, D.S., Győrffy, B., Lawrence, T., Dean, D.C., and Postigo, A. (2017). Tumor-associated macrophages (TAMs) depend on ZEB1 for their cancer-promoting roles. Embo J *36*, 3336–3355. https://doi.org/10.15252/embj.201797345.

13. Chen, L., Gibbons, D.L., Goswami, S., Cortez, M.A., Ahn, Y.H., Byers, L.A., Zhang, X., Yi, X., Dwyer, D., Lin, W., et al. (2014). Metastasis is regulated via microRNA-200/ZEB1 axis control of tumour cell PD-L1 expression and intratumoral immunosuppression. Nat. Commun. *5*, 5241. https://doi.org/10.1038/ncomms6241.

14. Shousha, W.G., Ramadan, S.S., El-Saiid, A.S., Abdelmoneim, A.E., and Abbas, M.A. (2019). Expression and clinical significance of SNAI1 and ZEB1 genes in acute myeloid leukemia patients. Mol. Biol. Rep. *46*, 4625–4630. https://doi.org/10.1007/s11033-019-04839-y.

15. Stavropoulou, V., Kaspar, S., Brault, L., Sanders, M.A., Juge, S., Morettini, S., Tzankov, A., Iacovino, M., Lau, I.J., Milne, T.A., et al. (2016). MLL-AF9 Expression in Hematopoietic Stem Cells Drives a Highly Invasive AML Expressing EMT-Related Genes Linked to Poor Outcome. Cancer Cell *30*, 43–58. https://doi.org/10.1016/j.ccell.2016.05.011.

16. Li, L., Feng, Y., Hu, S., Du, Y., Xu, X., Zhang, M., Peng, X., and Chen, F. (2021). ZEB1 serves as an oncogene in acute myeloid leukaemia via regulating the PTEN/PI3K/AKT signalling pathway by combining with P53. J. Cell Mol. Med. *25*, 5295–5304. https://doi.org/10.1111/jcmm.16539.

17. Mopin, A., Driss, V., and Brinster, C. (2016). A Detailed Protocol for Characterizing the Murine C1498 Cell Line and its Associated Leukemia Mouse Model. J. Vis. Exp. *116*, e54270. https://doi.org/10.3791/54270.

18. Tomida, M. (1995). Induction of differentiation of WEHI-3B D+ leukemic cells transfected with differentiation-stimulating factor/leukemia inhibitory factor receptor cDNA. Blood *85*, 217–221.

19. Geginat, J., Paroni, M., Kastirr, I., Larghi, P., Pagani, M., and Abrignani, S. (2016). Reverse plasticity: TGF-beta and IL-6 induce Th1-to-Th17-cell transdifferentiation in the gut. Eur. J. Immunol. *46*, 2306–2310. https://doi.org/10.1002/eji.201646618.

20. Vitali, C., Bassani, C., Chiodoni, C., Fellini, E., Guarnotta, C., Miotti, S., Sangaletti, S., Fuligni, F., De Cecco, L., Piccaluga, P.P., et al. (2015). SOCS2 Controls Proliferation and Stemness of Hematopoietic Cells under Stress Conditions and Its Deregulation Marks Unfavorable Acute Leukemias. Cancer Res. *75*, 2387–2399. https://doi.org/10.1158/0008-5472.CAN-14-3625.

21. Pirillo, C., Birch, F., Tissot, F.S., Anton, S.G., Haltalli, M., Tini, V., Kong, I., Piot, C., Partridge, B., Pospori, C., et al. (2022). Metalloproteinase inhibition reduces AML growth, prevents stem cell loss, and improves chemotherapy effectiveness. Blood Adv. *6*, 3126–3141. https://doi.org/10.1182/bloodadvances.2021004321.

22. Feng, S., Cen, J., Huang, Y., Shen, H., Yao, L., Wang, Y., and Chen, Z. (2011). Matrix metalloproteinase-2 and -9 secreted by leukemic cells increase the permeability of blood-brain barrier by disrupting tight junction proteins. PLoS One *6*, e20599. https://doi.org/10.1371/journal.pone.0020599.

23. Stritesky, G.L., Yeh, N., and Kaplan, M.H. (2008). IL-23 promotes maintenance but not commitment to the Th17 lineage. J. Immunol. *181*, 5948–5955. https://doi.org/10.4049/jimmunol.181.9.5948.

24. Remacle, J.E., Kraft, H., Lerchner, W., Wuytens, G., Collart, C., Verschueren, K., Smith, J.C., and Huylebroeck, D. (1999). New mode of DNA binding of multi-zinc finger transcription factors: deltaEF1 family members bind with two hands to two target sites. Embo J *18*, 5073–5084. https://doi.org/10.1093/emboj/18.18.5073.

25. Feldker, N., Ferrazzi, F., Schuhwerk, H., Widholz, S.A., Guenther, K., Frisch, I., Jakob, K., Kleemann, J., Riegel, D., Bönisch, U., et al. (2020). Genome-wide cooperation of EMT transcription factor ZEB1 with YAP and AP-1 in breast cancer. Embo J *39*, e103209. https://doi.org/10.15252/embj.2019103209.

26. Meidhof, S., Brabletz, S., Lehmann, W., Preca, B.T., Mock, K., Ruh, M., Schüler, J., Berthold, M., Weber, A., Burk, U., et al. (2015). ZEB1-associated drug resistance in cancer cells is reversed by the class I HDAC inhibitor mocetinostat. EMBO Mol. Med. *7*, 831–847. https://doi.org/10.15252/emmm.201404396.

27. Hackl, H., Steinleitner, K., Lind, K., Hofer, S., Tosic, N., Pavlovic, S., Suvajdzic, N., Sill, H., and Wieser, R. (2015). A gene expression profile associated with relapse of cytogenetically normal acute myeloid leukemia is enriched for leukemia stem cell genes. Leuk. Lymphoma *56*, 1126–1128. https://doi.org/10.3109/10428194.2014.944523.

28. Corradi, G., Bassani, B., Simonetti, G., Sangaletti, S., Vadakekolathu, J., Fontana, M.C., Pazzaglia, M., Gulino, A., Tripodo, C., Cristiano, G., et al. (2022). Release of IFN-gamma by acute myeloid leukemia cells remodels bone marrow immune microenvironment by inducing regulatory T cells. Clin. Cancer Res. *28*, 3141–3155. https://doi.org/10.1158/1078-0432.CCR-21-3594.

29. Almotiri, A., Alzahrani, H., Menendez-Gonzalez, J.B., Abdelfattah, A., Alotaibi, B., Saleh, L., Greene, A., Georgiou, M., Gibbs, A., Alsayari, A., et al. (2021). Zeb1 modulates hematopoietic stem cell fates required for suppressing acute myeloid leukemia. J. Clin. Invest. *131*, e129115. https://doi.org/10.1172/JCI129115.

30. Musuraca, G., De Matteis, S., Napolitano, R., Papayannidis, C., Guadagnuolo, V., Fabbri, F., Cangini, D., Ceccolini, M., Giannini, M.B., Lucchesi, A., et al. (2015). IL-17/IL-10 double-producing T cells: new link between infections, immunosuppression and acute myeloid leukemia. J. Transl. Med. *13*, 229. https://doi.org/10.1186/s12967-015-0590-1.

31. Vitali, C., Tripodo, C., and Colombo, M.P. (2015). MEF2C and SOCS2 in stemness regulation. Oncoscience *2*, 936–937. https://doi.org/10.18632/oncoscience.279.

32. Subramanian, K., Dierckx, T., Khouri, R., Menezes, S.M., Kagdi, H., Taylor, G.P., Farre, L., Bittencourt, A., Kataoka, K., Ogawa, S., and Van Weyenbergh, J. (2019). Decreased RORC expression and downstream signaling in HTLV-1-associated adult T-cell lymphoma/leukemia uncovers an antiproliferative IL17 link: A potential target for immunotherapy? Int. J. Cancer *144*, 1664–1675. https://doi.org/10.1002/ijc.31922.

33. Thol, F., and Ganser, A. (2020). Treatment of Relapsed Acute Myeloid Leukemia. Curr. Treat. Options Oncol. *21*, 66. https://doi.org/10.1007/s11864-020-00765-5.

34. Terry, S., Savagner, P., Ortiz-Cuaran, S., Mahjoubi, L., Saintigny, P., Thiery, J.P., and Chouaib, S. (2017). New insights into the role of EMT in tumor immune escape. Mol. Oncol. *11*, 824–846. https://doi.org/10.1002/1878-0261.12093.

35. Dongre, A., Rashidian, M., Reinhardt, F., Bagnato, A., Keckesova, Z., Ploegh, H.L., and Weinberg, R.A. (2017). Epithelial-to-Mesenchymal Transition Contributes to Immunosuppression in Breast Carcinomas. Cancer Res. *77*, 3982–3989. https://doi.org/10.1158/0008-5472.CAN-16-3292.

36. Plaschka, M., Benboubker, V., Grimont, M., Berthet, J., Tonon, L., Lopez, J., Le-Bouar, M., Balme, B., Tondeur, G., de la Fouchardière, A., et al. (2022). ZEB1 transcription factor promotes immune escape in melanoma. J. Immunother. Cancer *10*, e003484. https://doi.org/10.1136/jitc-2021-003484.

37. Carvalho, B.S., and Irizarry, R.A. (2010). A framework for oligonucleotide microarray preprocessing. Bioinformatics *26*, 2363–2367. https://doi.org/10.1093/bioinformatics/btq431.

38. Leek, J.T., and Storey, J.D. (2007). Capturing heterogeneity in gene expression studies by surrogate variable analysis. PLoS Genet. *3*, 1724–1735. https://doi.org/10.1371/journal.pgen.0030161.

39. Ritchie, M.E., Phipson, B., Wu, D., Hu, Y., Law, C.W., Shi, W., and Smyth, G.K. (2015). limma powers differential expression analyses for RNA-sequencing and microarray studies. Nucleic Acids Res. *43*, e47. https://doi.org/10.1093/nar/gkv007.

40. Subramanian, A., Tamayo, P., Mootha, V.K., Mukherjee, S., Ebert, B.L., Gillette, M.A., Paulovich, A., Pomeroy, S.L., Golub, T.R., Lander, E.S., and Mesirov, J.P. (2005). Gene set enrichment analysis: a knowledge-based approach for interpreting genome-wide expression profiles. Proc. Natl. Acad. Sci. USA *102*, 15545–15550. https://doi.org/10.1073/pnas.0506580102.

41. Miller, J.A., Cai, C., Langfelder, P., Geschwind, D.H., Kurian, S.M., Salomon, D.R., and Horvath, S. (2011). Strategies for aggregating gene expression data: the collapseRows R function. BMC Bioinf. *12*, 322. https://doi.org/10.1186/1471-2105-12-322.

42. Phipson, B., Lee, S., Majewski, I.J., Alexander, W.S., and Smyth, G.K. (2016). Robust Hyperparameter Estimation Protects against Hypervariable Genes and Improves Power to Detect Differential Expression. Ann. Appl. Stat. *10*, 946–963. https://doi.org/10.1214/16-AOAS920.

STAR★METHODS

KEY RESOURCES TABLE

REAGENT or RESOURCE	SOURCE	IDENTIFIER
Antibodies		
Monoclonal rat anti-mouse CD11b (clone M1/70)	BD	cat#563402; RRID:AB_2738184
Monoclonal mouse anti-human CD66b (clone G10F5)	BD	cat#562940; RRID:AB_2737906
Monoclonal mouse anti-human CD15 (clone HI98)	BD	cat#563838; RRID:AB_2738444
Monoclonal mouse anti-human CD16 (clone 3G8)	BD	cat#561248; RRID:AB_10612010
Monoclonal mouse anti-human CD14 (clone M5E2)	BD	cat#555397; RRID:AB_395798
Monoclonal rat anti-mouse CD71 (clone M-A712)	BD	cat#748082; RRID:AB_395918
Monoclonal mouse anti-human HLA-DR (clone LN3)	eBioscience	cat#47-9956-42; RRID:AB_1963603
Monoclonal mouse anti-human CD33 (clone HIM3-4)	Invitrogen	cat#12-0339-42; RRID:AB_10855031
Monoclonal mouse anti-human CD10 (clone HI10a)	Biolegend	cat#312228; RRID:AB_2565878
Monoclonal mouse anti-human CD3 (clone HIT3a)	BD	cat#740961; RRID:AB_2740586
Monoclonal mouse anti-human CD8 SK1 (clone SK1)	BD	cat#563919; RRID:AB_2722546
Monoclonal mouse anti-human Lineage Cocktail 1	BD	Cat#340546; RRID:AB_400053
Monoclonal rat anti-mouseCD45 (clone 30F11)	eBioscience	Cat #14-0451-82; RRID:AB_467251
Monoclonal hamster anti-mouse CD3 (clone 145-2C11)	BD	Cat #564379; RRID:AB_2738780
Monoclonal rat anti-mouse CD45R (clone RA3-6B2)	BD	Cat #552094; RRID:AB_394335
Monoclonal rat anti-mouse CD115 (clone AFS98)	Biolegend	Cat #25-1152-82; RRID:AB_2573386
Monoclonal rat anti-mouse CD18 (clone M18/2)	BD	Cat #744597; RRID:AB_2742346
Monoclonal rat anti-mouse CD107b (clone M3/84)	eBioscience	Cat #12-5989-82; RRID:AB_466103
Monoclonal rat anti-mouse Ly6G (clone 1A8)	BD	Cat #562737; RRID:AB_2737756
Monoclonal rat anti-mouse Ly6C (clone AL-21)	BD	Cat #563011; RRID:AB_2737949
Monoclonal rat anti-mouse CD8a (clone 53–6.7)	BioLegend	Cat #100714; RRID:AB_312753
Monoclonal rat anti-mouse CD4 8clone GK1.5)	eBioscience	Cat #12-0041-81; RRID:AB_465505
Monoclonal rat anti-mouse CD134 (OX-86)	eBioscience	Cat #17-1341-82; RRID:AB_10717260
Monoclonal rat anti-mouse CD25 (clone PC-61)	BD	Cat #564021; RRID:AB_2738547
Monoclonal rat anti-mouse, human FOXP3 (clone FJK-16s)	eBioscience	Cat #45-5773-82; RRID:AB_914351
Monoclonal mouse anti-human Ki-67 (B56)	BD	Cat #561126; RRID:AB_10611874
Rat anti-mouse CD279 (clone RMP1-30)	BD	Cat #748268; RRID:AB_2872696
Rat anti-mouse TNF-α (clone MP6-XT22)	BD	Cat #563386; RRID:AB_2738172
Rat anti-mouse IL-17a (clone TC11-18H10)	BioLegend	Cat #506910; RRID:AB_536012
Mouse anti-mouse CD366 (clone RMT3-23)	BD	Cat #747626; RRID:AB_2744192
Monoclonal mouse anti mouse/rat/rabbit/ human β−actin	Sigma	Cat #A1978; RRID:AB_476692
Polyclonal rabbit anti mouse/human/rat CD3	Abcam	Cat #ab5690; RRID:AB_305055
Polyclonal goat anti-human IL-17	R&D	Cat #AF-317-SP; RRID:AB_354463
Monoclonal mouse anti-human ZEB1 (clone OTI3G6)	Abcam	Cat #ab18905; RRID:AB_286
Polyclonal rabbit anti-human ZEB1(E2G6Y)	Cell Signaling Technology	Cat #70512; RRID:AB_2935802
Polyclonal rabbit anti-human ZEB1	Genetex	Cat #GTX105278; RRID:AB_11162905
Monoclonal rabbit anti human H3K27me3 (clone G.299.10)	Thermo Fisher Scientific	Cat #MA5-11198; RRID:AB_11000749
Polyclonal rabbit anti-human H3K4me3	Thermo Fisher Scientific	Cat #PA5-120809, RRID:AB_2914381

(*Continued on next page*)

Continued

REAGENT or RESOURCE	SOURCE	IDENTIFIER
Mouse monoclonal H3K27ac	Thermo Fisher Scientific	Cat #MA5-23516, RRID:AB_2608307
Histone H3 (clone D2B10)	Cell Signaling Technology	Cat #4620, RRID:AB_1904005
Chemicals, Peptides, and Recombinant Proteins		
InVivoMAb anti-mouse/rat IL-17A	BioXCell	Cat #BE0246
InVivoMAb polyclonal Armenian hamster IgG	BioXCell	Cat #BE0091
InVivoMAb anti-mouse IL-23	BioXCell	Cat #BE0313
Recombinant human IL-17A	Peprotech	Cat #200-17
Recombinant mouse IL-17A	Peprotech	Cat #200-17
Cell Proliferation dye	eFluor670	Cat #65-0840-85
Cytosine β-D-arabinofuranoside	Merck	Cat #C1768
rowhead**Critical commercial assays**		
SimpleChIP Enzymatic Chromatin IP kit	Cell Signaling Technologies	Cat ##9003
Transcription Factor Buffer Set	BD	Cat #562574
Deposited data		
Raw and analyzed data	This paper	GEO:GSE192473
Experimental models: Cell lines		
Mouse: C1498	ATCC	Cat #TIB-49
Mouse: *WEHI-3B*	ATCC	Cat #TIB-68
Human: K562	ATCC	Cat #CCL-243
Oligonucleotides		
Primers for qPCR are Listed in Table S3		
Primers for CHIP-PCR are Listed in Table S4		
Recombinant DNA		
pLKO.1-shZEB1-565 (MISSION®)	Merck	Cat #TRCN0000017565
pLKO.1-shZEB1-631 (MISSION®)	Merck	Cat #TRCN0000364631
pLKO.1-puro-CMV-TurboGFP™ Positive Control Plasmid DNA (MISSION®)	Merck	Cat #SHC003
pGFP-C-shLenti	Origine	Cat # TL513177V
Software and algorithms		
Prism version 9	GraphPad	https://www.graphpad.com/updates/prism-900-release-notes
FlowJo version 10	BD	https://www.flowjo.com/solutions/flowjo/downloads

RESOURCE AVAILABILITY

Lead contact

Further information and request should be directed to and will be fulfilled by the corresponding author Sabina Sangaletti (sabina.sangaletti@istitutotumori.mi.it)

Materials availability

This study did not generate unique reagents.

Data and code availability

- Gene expression data included in this study are available in GEO accession number GSE192473. All other original data reported in this paper are available from the lead contact upon request.
- This paper does not report original code.
- Any additional information required to reanalyze the data reported in this work paper is available from the lead contact upon request.

EXPERIMENTAL MODEL AND STUDY PARTICIPANT DETAIL

Cell lines

The C1498 cell line, a murine AML cell line isolated from a leukemic 10-month-old C57BL/6 (H-2b) was purchased from ATCC, while the WEHI-3B murine myelomonocyte cell line syngeneic to BALB/c mice was purchased from Sigma Aldrich (Merck, 86013003). K562 are a human erythroleukemia cell line isolated from the bone marrow of a 53-year-old patient. Cells were cultured in DMEM (Dulbecco's modified Eagle's medium) or RPMI-1640 (Thermo Fisher Scientific) supplemented with 10% fetal bovine serum (FBS; Thermo Fisher Scientific), 1% antibiotics (Thermo Fisher Scientific), 2mM glutamine, 1mM sodium pyruvate, 1mM HEPES and 1X Minimum Essential Medium (MEM) Non-Essential Amino Acids Solution, in a humidified atmosphere containing 5% CO_2 at 37°C.

Animal models

Animal studies were approved by Institutional Committee for Animal Welfare and by the Italian Ministry of Health and performed in accordance with national law D.lgs 26/2014 (authorization n. 781/2018-PR). For the experiments involving C1498 intra-bone (i.b.) injection, at day 0, $2x10^5$ Scr-C1498 or shZeb1-C1498 cells were injected into the tibia of immunocompetent 8-weeks old female mice. After 34 days, mice were sacrificed.

For experiments using the IL-17A-neutralizing antibody, animals were injected with $5x10^5$ *Zeb1*-competent or silenced C1498. After 3 days, they were randomized. IL-17A–neutralizing or isotype control Ab (50μg/mouse) were injected i.p. twice a week. Mice were sacrificed after 30 days and BM and liver were explanted for further FACS analyses.

Experiments with AraC were performed administering the drug at day 7, 9, 12, 14 after ib injection. In all the *in vivo* studies cohorts of mice were euthanized for FACS analysis if they reached the humane endpoints (https://www.humane-endpoints.info): loss of >15% body weight for up to 72 h (score 6), dyspnea (score 4) diarrhea (score 2) blood stool (score 6) or signs of pain and distress including poor grooming and decreased activity, light moderate severe lameness (score 1, 4 and 6). With a score > o = 6 mice were euthanized.

Patients

IHC analysis was performed on BM biopsies from retrospective AML cases (n = 26) from the University of Palermo (Protocol 443/1/10/18, authorization number 09/2018). No clinical information concerning disease features and patients outcome are currently available.

METHOD DETAILS

Flow cytometry analysis

For the intracellular staining we used the the Foxp3/Transcription Factor Staining Buffer Kit (Tonbo Biosciences). Samples were analyzed with the FACSCelesta flow cytometer equipped with FACSDiva software (v 6.0) (Becton Dickinson). Flow cytometry data analyses were performed using FlowJo software (v10.2).

Quantitative immunolocalization analyses

For immunohistochemistry (IHC), human and murine bone marrow samples were fixed in 10% buffered formalin, decalcified using an EDTA-based buffer, and paraffin-embedded. Four micrometers tissue sections were deparaffinized and rehydrated. Novocastra Epitope Retrieval Solution (pH9) was used to unmask antigens in a thermostatic bath at 98°C for 30 min. Subsequently, the sections were brought to room temperature and washed in PBS. After neutralization of the endogenous peroxidases with 3% H_2O_2 and Fc-blocking by 0.4% casein in PBS (Novocastra), the sections were incubated with primary antibodies listed in the key resources table. IHC staining was developed using the Novolink Polymer Detection Systems (Novocastra) or IgG-Peroxidase specific secondary antibody (Sigma Aldrich) and DAB (3,3′-diaminobenzidine) as substrate chromogen. Anti-mouse and anti-goat (Alexa Fluor 488 and 568 conjugate) secondary antibodies were used for immunofluorescence (IF) and DAPI (4′,6-diamidin-2-fenilindolo) for nuclei visualization. Slides were analyzed under a Zeiss Axioscope A1 microscope equipped with four fluorescence channels widefield IF. Microphotographs were collected using a Zeiss Axiocam 503 Color digital camera with the Zen 2.0 Software (Zeiss). Slide digitalization was performed using an Aperio CS2 digital scanner (Leica Biosystems) with the ImageScope software (Aperio ImageScope version 12.3.2.8013, Leica Biosystems). Quantitative analyses of IHC stainings were performed by calculating the average percentage of positive signals in five separate fields at medium-power magnification (X200) using the Nuclear Hub Image Analysis package and the result was expressed as a percentage.

Extramedullary disease evaluation

Livers from i.b. injected mice either with Zeb1-expressing or -silenced C1498 cells were explanted after 34 days, washed in PBS and fixed in 10% neutral buffered formalin overnight before embedding in paraffin. Four-micrometers-thick tissue sections were deparaffinized using xylol and firstly rehydrated in 100% ethanol for 5 min. Then, sections were incubated in 95%, 80%, 50% ethanol for 5 min and finally washed in distillated water. Sections were incubated with hematoxylin for 8 min and then washed. Eosin was added to the tissue sections for 3 min and then washed. The stained sections were dehydrated in 70% ethanol for 2 min, 100% ethanol for

2 min and finally in xylol twice for 5 min. Sections were mounted using Eukitt (Biosigma). Infiltrated areas were then quantified using Leica software. For flow cytometry analysis, livers were mechanically smashed in DMEM with 10% FBS and then filtered through 70 μm cell strainer. Red blood cells were lysed using a solution of Ammonium-Chloride-Potassium lysing Buffer (ACK). If necessary a second step of filtration was made prior analysis by flow cytometry to avoid clogging issues.

Immunoblotting

40μg of the total protein lysate was separated on 8 or 12% SDS–polyacrylamide gel electrophoresis under reducing conditions and transferred onto nitrocellulose membranes (Amersham, Biosciences). Following blocking with 5% bovine serum albumin (BSA) and 0.1% Tween 20, the membranes were incubated with the antibodies listed in the key resource table (1:1000 dilution) overnight at 4°C. After rinsing in tris-buffered saline (TBS) 0.1% Tween 20, membranes were incubated with horseradish peroxidase conjugated goat anti-rabbit secondary antibodies (Thermo Scientific; 1:2000) and reactions were visualized with the Western BLoT Quant HRP Substrate (TakaraBio).

Invasion assay

$2.5x10^5$ C1498 cells either with and without silenced *Zeb1* expression were resuspended in 200μL of serum-free high glucose DMEM and placed onto the upper chamber of a 24-well Transwell plate (5-μm pore size) coated with growth factor reduced matrigel (1 mg/mL). 750μL of high glucose DMEM containing 10% FBS was added into the lower chamber. After 24 h at 37°C and 5% CO_2, top chambers, containing non-migrated cells were removed, while cells that migrated into the lower chamber were counted using the all-in-one digital inverted fluorescence microscope (EVOS fl – advance microscopy group). Five randomly selected fields per well were counted.

Proliferation assay

To assess the proliferation of Zeb1-expressing or -silenced cells, we used the colorimetric XTT assay. This test is based on the cleavage of tetrazolium salts added to the culture medium and allow the evaluation of cell viability and proliferation. Briefly, 10^4 cells were seeded in a 96-well plate in 100 mL of DMEM 10% FBS for four different time point, termed t_0, t_{24}, t_{48} and t_{72}. For each time point, plated cells were incubated with 50μL XTT labeling mixture per well and incubate for 4h at 37°C and 5% CO_2. Absorbance of the formazan products was measured at 450nm Tecan's Spark Microplate reader, while the reference wavelength was read at 670nm.

In vitro suppression assay

4×10^5 naive C57Bl/6 splenocytes were labeled with CFSE (Carboxyfluorescein Succinimidyl ester; 10mM, SIGMA Aldrich) or with the eBioscience Proliferation Dye eFluor670 and co-cultured with irradiated (3Gy) C1498 Zeb1-expressing or -silenced cells at different ratio in presence of 2 μg/ml of soluble anti-CD3 and 1 μg/ml of anti-CD28 to activate lymphocytes. Each sample was seeded in triplicate. Proliferation of CD4 and CD8 T cells has been assessed after 48h by flow cytometry evaluating CFSE/proliferation dye dilution in the $CD4^+$ and $CD8^+$ gated populations.

Human transcriptomic data analysis

For each experiment raw data were imported in R software, background corrected, log transformed and normalized using Robust Multichip Average (RMA) method from oligo package.[37] Multiple probes representing the same gene were collapsed by selecting the probe with the highest variance across samples through the collapse Rows function in the WGCNA package. For DEG analysis, data from GSE6891, GSE12417, GSE15434, GSE16015 and GSE37642, profiled with Human Genome U133 Plus 2.0 Array were selected. Datasets were merged together by matching probes and batch effect was removed through ComBat function from sva package.[38] Samples were separated into two groups according to the median level of ZEB1 expression and DEGs were calculated using the limma package[39] then p values were adjusted for multiple tests using the Benjamini–Hocheberg FDR. Genes with an FDR <0.05 were considered statistically significant. Pre-ranked GSEA [40] was performed to calculate which hallmark pathways were significantly up or down modulated. Selected genes where charted through a boxplot.

Three datasets including information on survival, GSE6891 (Human Genome U133 Plus 2.0 Array), GSE37642 and GSE12417 (Human Genome U133A Array), were used for molecular and clinical correlation studies. Survival analysis was first performed in each dataset independently and then merging the datasets together as described above. After data quality control, normalization and correction, samples were separated into two groups according to the median level of ZEB1 expression, the Kaplan Meier curves were plotted and the statistical significance was assessed performing a log rank test.

To assess the differences between diagnosis and relapse we exploited the data from GSE66525, consisting of 11 samples pre and post-chemotherapy. Pre-processed RMA normalized data were downloaded from NCBI Gene Expression Omnibus (GEO) repository and multiple probes representing the same gene were collapsed selecting the probe with the highest variance across samples. Limma package was used to calculate differentially expressed genes and selected genes where charted through a boxplot.

ChIP-qPCR

ChIP was performed on previously cross-linked K562 cells. Briefly, 10^7 cells were fixed with 1% formaldehyde and digested with Micrococcal Nuclease into fragments <900-bp following manufacturer's recommendation (SimpleChIP Enzymatic Chromatin IP

kit, CST). Clarified cell extracts (0.5 mL aliquots) were incubated o/n with antibodies to ZEB1 (1 μg, N2C1, Genetex); H3K27me3 (0.5 μg, clone G.299.10), H3K4me3 (2.5 μg, polyclonal #49–1005), H3K27ac (2 μg, mouse monoclonal) from Invitrogen; histone H3 (10 μL, D2B12) and normal rabbit IgG (1 μL) from CST. Antibody-chromatin complexes were spun down following 3 h incubation with protein G magnetic beads and eluted strictly following protocol instructions. Cross-reversal of chromatin and protein digestion with Proteinase K were achieved at 65°C for 3 h, and purified DNA fragments were opportunely processed by qPCR with primers encompassing target loci (Figures S5–S7). Amplicon enrichment by specific antibodies and IgG were normalized to nucleosomal histone H3, as an internal referral of total chromatin content per sample. Oligonucleotides are provided in Table S4.

Stable gene-silencing

Lentiviral Particles were purchased from OriGene Technologies (catalog number TL513177V). Two specific constructs (“seq-C” and “seq-D″) were tested for efficiency compared to a negative control construct (“Scr”). For ZEB1 stable silencing in human K562 cells, we used the Mission Lentivirus Transduction Particles (pLKO.1-shZEB1-565 - TRCN0000017565 and pLKO.1-shZEB1-631 - TRCN0000364631), purchased from Sigma-Aldrich. A non-target (Scramble - SHC003) sequence was used as negative control.

Transient gene-silencing

Silencer pre-designed siRNA SOCS2 sequences were purchased from Ambion (Life Technologies). A scramble and 3 sequences were used (see key resource Table). For the transient silencing C1498 cells were maintained 72h with 20μm of each sequence. The invasion assay was performed starting at 48h.

Total RNA extraction, reverse transcription, and quantitative polymerase chain reaction (qPCR)

Total RNA was extracted using the Quick RNA micro prep kit (Zymo Research) and subsequently quantified by NanoDrop 2000c Spectrophotometer (Thermo Scientific). cDNA was generated using the high capacity Reverse Transcriptase kit (Applied Biosystems) according to the manufacturer’s instructions. Values were normalized to internal control (β-Actin) using the ΔCT method. For IL-17A stimulation experiments, $5x10^4$ human and murine cell lines expressing or silenced were treated for 7 days with 50 ng/mL rIL-17A. Untreated cells were used as control. ΔΔCT results are shown. rIL-17A-stimulated cells were normalized to untreated cells. Oligonucleotides are provided in Table S3.

Gene expression profile of mouse cell lines

Gene expression profiles were established by Thermo Fisher Mouse Clariom S Assay. RNA labeling, processing, and hybridization were performed according to manufacturer’s instructions, and microarrays were scanned with the Gene Chip System 3000 scanner. Raw data were pre-processed using the sst-RMA algorithm implemented in the Transcriptome Analysis Console software (Thermo Fisher). Downstream analyses were performed on pre-processed data using R software. Multiple probes representing the same gene were collapsed by selecting the probe with the highest variance across samples through the collapseRows function in the WGCNA package.[41] Differentially expressed genes (DEG) were identified using limma package.[42] P-values were adjusted for multiple testing using the Benjamini–Hocheberg false discovery rate (FDR). Genes with an FDR<0.05 were considered statistically significant. Gene set enrichment analysis (GSEA[40]) was carried out in pre-ranked mode, according to the limma t-statistic, using the hallmark gene set collection from the MSigDB database (http://software.broadinstitute.org/gsea/msigdb/index.jsp). Gene sets with an FDR<0.05 were considered statistically significant.

QUANTIFICATION AND STATISTICAL ANALYSIS

Statistical analyses have been performed with GraphPad Software (Prism 8). The statistic applied to every single experiment is shown in the relative figure legend. Parametric and non-parametric analysis (Student t test, Mann-Whitney test) have been applied according to data distribution. A one-way ANOVA analysis with Tukey’s or Dunnett’s multiple comparison has been applied according to multiple comparison.